Petroleum Science 22 (2025) 998–1020

Contents lists available at ScienceDirect

Petroleum Science

journal homepage: www.keaipublishing.com/en/journals/petroleum-science

Original Paper

Formation mechanism and reservoir quality evaluation in tight sandstones under a compressional tectonic setting: the Jurassic Ahe Formation in Kuqa Depression, Tarim Basin, China

Dong Li [a, b, *], Gui-Wen Wang [a, b, **], Kang Bie [c, d], Jin Lai [a, b], De-Wen Lei [e], Song Wang [a, b], Hai-Hua Qiu [c, d], Hong-Bo Guo [c, d], Fei Zhao [a, b], Xing Zhao [a, b], Qi-Xuan Fan [a, b]

[a] National Key Laboratory of Petroleum Resources and Engineering, China University of Petroleum (Beijing), Beijing, 102249, China
[b] College of Geosciences, China University of Petroleum (Beijing), Beijing, 102249, China
[c] Research Institute of Petroleum Exploration and Development, Tarim Oilfield Company, CNPC, Korla, 841000, Xinjiang, China
[d] R&D Center for Ultra-Deep Complex Reservoir Exploration and Development, CNPC, Korla, 841000, Xinjiang, China
[e] Exploration Division, Xinjiang Oilfield Company, CNPC, Karamay, 834000, Xinjiang, China

ARTICLE INFO

Article history:
Received 8 July 2024
Received in revised form
6 October 2024
Accepted 27 December 2024
Available online 30 December 2024

Edited by Jie Hao

Keywords:
Reservoir quality
The Ahe formation
Sedimentation
Diagenesis
In situ stress
Fracture

ABSTRACT

The northern structural belt of Kuqa Depression is adjacent to the South Tianshan orogenic belt, which are characterized by complex geological conditions. The reservoir quality of the Jurassic Ahe Formation is controlled by sedimentation, diagenesis, and tectonics, and show complex pore structure and strong heterogeneity, thereby hindering effective natural gas exploration and development. Core, thin sections, cathodoluminescence (CL), scanning electron microscopy (SEM), conventional well logs and image logs are used to characterize the petrological characteristics and pore systems. Then a comprehensive analysis integrating sedimentation, diagenesis, and tectonics is performed to unravel the reservoir formation mechanism and distribution of reservoir quality. Results show that reservoir properties are generally environmentally selective. Coarse grained sandbodies (gravelly sandstones) formed in high depositional-energy have the best physical properties, while fine sandstone and mudstone with low depositional energy is easily to be tightly compacted, and have poor reservoir quality. Porosity usually decreases with compaction and cementation, and increases due to dissolution. Clay minerals filling pores result in a deterioration of the pore structure. Microfracture formed by fracturing can connect the matrix pores, effectively improving the reservoirs' permeability. The differential distribution of fractures and in-situ stress plays an important role in modifying reservoir quality. The in-situ stress has obvious control over the matrix physical properties and fracture effectiveness. The matrix physical properties are negatively correlated with the value of horizontal stress difference ($\Delta\sigma$). As the value of $\Delta\sigma$ increases, the pore structure becomes more complex, and the macroscopic reservoir quality becomes poor. The smaller the strike divergence between the natural fracture and SH_{max}, the lower the value of $\Delta\sigma$ in the fracture layers is, and the better the fracture effectiveness is. Under the control of ternary factors on the reservoir, sedimentation-diagenesis jointly affect the matrix reservoir quality, while fractures and in-situ stress caused by tectonism affect the permeability and hydrocarbon productivity of the reservoir. Affected by ternary factors, reservoir quality and hydrocarbon productivity show obvious differences within the various structural location. Reservoir quality in tight sandstones can be predicted by integrating sedimentation, diagenesis, and tectonics (fracture and in-situ stress) in a compressional tectonic setting like Kuqa Depression. The research results will provide insights into the efficient exploration of oil and gas in Kuqa Depression as well as similar compressional tectonic settings elsewhere.

1. Introduction

Understanding the control and distribution of reservoir quality is critical for commercial production of oil and gas, especially

* Corresponding author.
** Corresponding author.
E-mail addresses: lidongcupb@163.com (D. Li), wanggw@cup.edu.cn (G.-W. Wang).

https://doi.org/10.1016/j.petsci.2024.12.026

unconventional resources (Bloch et al., 2002; Higgs et al., 2007). Tight sandstones show huge hydrocarbon exploration potential (Zou et al., 2012). Reservoir quality in tight sandstones is a comprehensive reflection of initial sediment composition, and subsequent diagenetic alterations (Ramm, 2000; Ozkan et al., 2011; Zhang et al., 2015; Higgs et al., 2017) as well as tectonic modification (formation, attributes of fracture and in-situ stress field) (Laubach et al., 2010; Almansour et al., 2020; Del Sole et al., 2020), which also affect subsequent diagenetic fluid activity and participate in diagenesis (Nguyen et al., 2013; Vandeginste et al., 2012; Rodrigues et al., 2021). In terms of genetic mechanism of reservoir quality, the sandstones with complex structure patterns and concentrated stress (foreland basin) are controlled by the coupling of sedimentation, diagenesis and tectonics, since tectonic activity and in-situ stress fields also act as significant reservoir quality modifying factors (Lan et al., 2010). The differential distribution of fractures and in-situ stress plays important roles in modifying the formation and distribution of high-quality reservoir (Zeng et al., 2020; Li et al., 2021).

The northern structural belt of Kuqa Depression has favorable petroleum geological conditions (Lu et al., 2014; Shen et al., 2017; Wei et al., 2022). Nevertheless, due to its proximity to the South Tianshan orogenic belt, the geological conditions are intricate since the in-situ stress are intense, and the rocks are heavily fractured. Sandstone reservoirs have undergone complex diagenetic evolution and tectonic modifications in a long historical period (Ju and Wang, 2018; Tang et al., 2021; Wang K. et al., 2022). The sandstone reservoirs are jointly influenced by multiple factors, including sedimentation, diagenesis, and tectonics, exhibiting intricate pore structures and strong heterogeneity (Zhang et al., 2020; Wang et al., 2020). The characteristics and formation mechanisms of the tight sandstone reservoirs remain unclear in a compressional tectonic setting, hindering the successful exploration and efficient development of natural gas (Lu et al., 2014).

Facing the above challenges, many scholars have focused on sedimentary facies and analyzed the impact of sandbody scale, grain size and shale content on reservoir quality under different hydrodynamic energies (Bjørlykke, 2014; Zhang et al., 2020; Radwan et al., 2021; Feng et al., 2024). In addition, the influence of diagenetic processes, diagenetic minerals, and diagenetic facies on reservoir properties and pore systems are also analyzed (Henares et al., 2014; Jiang et al., 2023). In recent years, with the acceleration of integration of geological engineering in the oil and gas industry, scholars such as Qiqiang Ren and Lianbo Zeng have carried out a series of related studies on the transformation of reservoirs by structural stress (strain) (Zeng et al., 2010; Li et al., 2021; Ren et al., 2024), including reservoir pore changes caused by tectonics (Shi et al., 2020; Rodrigues et al., 2021), as well as the formation, distribution, and quantitative prediction of tectonic fractures (Brandes and Tanner, 2020; Ren et al., 2020; Zeng et al., 2023). Most of the above studies evaluate reservoir quality only from a single perspective. Now, for tight sandstone reservoirs under strong stress fields, little systematic work has comprehensively integrated sedimentation, diagenesis, and tectonics, making it difficult to comprehensively reflect the reservoir formation mechanism. Thus, the effects of sedimentation, diagenesis and tectonics on the petrophysical properties of tight sandstone reservoirs should be discussed. The reservoir formation mechanism is revealed from the perspective of “three-element reservoir control” (sedimentology, diagenesis and tectonics), with the aim of unravelling the differential distribution of reservoir quality. This work has practical applications and scientific significance in Kuqa Depression as well as similar compressional tectonic settings elsewhere.

2. Geological settings

The Kuqa Depression is a Mesozoic to Cenozoic foreland depression controlled by the India-Asia plate collision located in the northern Tarim Basin (Jia, 2007). As the transition zone between the South Tianshan orogenic belt and the North Tarim uplift (Feng et al., 2018; Lai et al., 2023), the Kuqa Depression has experienced a long and complex evolutionary history (Ju and Wang, 2018). It mainly includes three tectonic evolution stages: compression stage during early Permian-Early Triassic, extension during Jurassic–Paleogene, and a rejuvenated foreland basin stage since Neogene (Neng et al., 2018). The complex and multiple tectonic evolutions resulted in the present tectonic configuration (Fig. 1(a)) (Li et al., 2022).

The study area is located in the northern margin of the Kuqa Depression. The strata are generally higher in the north and lower in the south. Large numbers of thrust faults and fault related folds are formed on the slope (Wang Q. et al., 2022; Wei et al., 2022) (Fig. 1(b)). The Jurassic Ahe Formation is unconformably overlying the Upper Triassic Taqikelike Formation (T_3t) and conformably underlying Lower Jurassic Yangxia Formation (T_1y) with a thickness of 260–280 m (Fig. 2) (Wei et al., 2022). The Ahe Formation was deposited in a braided deltaic plain depositional setting, and the lithologies are dominated by grayish-white gravelly sandstone, medium-coarse grained sandstones interbedded with thinly laminated conglomerate and mudstone (Feng et al., 2018; Li et al., 2022).

The Middle-Upper Triassic lacustrine mudstones and Middle-Lower Jurassic coal-bearing formation widely distributed in the Kuqa Depression are thought to be the primary hydrocarbon source rocks (Shen et al., 2017). In addition, the Middle-Lower coal-bearing formation is not only source rock but also high-quality regional cap rock (Lu et al., 2014). As a reservoir, the Jurassic Ahe Formation is sandwiched between two sets of hydrocarbon rocks, forming a “sandwich” structure of the source and reservoir assemblage (Fig. 2). The discovery of YN2 and DX1 gas pools shows that the Jurassic Ahe formation of the northern structural belt has a favorable oil and gas display and exploration prospect (Tang et al., 2021; Wang Q. et al., 2022).

3. Data and methods

3.1. Samples

Cores were taken from 10 cored wells in Kuqa Depression. Core surfaces were scanned for 360° to better record lithology, sedimentary structures as well as natural fractures. Helium porosity and permeability tests were performed on 546 core plug samples. Thin sections (30 μm in thickness) impregnated with blue-dye or red-dye resin were used to detect pore spaces. Also the composition and texture (framework grains, grain size, sorting), and diagenetic minerals and textures were detected using thin sections. An optical cathodoluminescence (CL) microscope was used to differentiate various types of carbonate minerals. Scanning electron microscopy (SEM) was used to detect the various types of clay minerals and recognize the micropores (<10 μm) within clay minerals. A total of 150 representative samples using freshly broken surfaces coated with carbon were observed in a Quanta 200 SEM equipment. Mercury Injection Capillary Pressure (MICP) analysis was conducted on the core plug samples to measure capillary pressure curves, and obtain capillary parameters (Lai et al., 2018; Su et al., 2024). A mercury porosimeter with a maximum injection pressure of 180.29 MPa was used to force mercury to invade into pore throat systems and measure the volume of mercury entered into

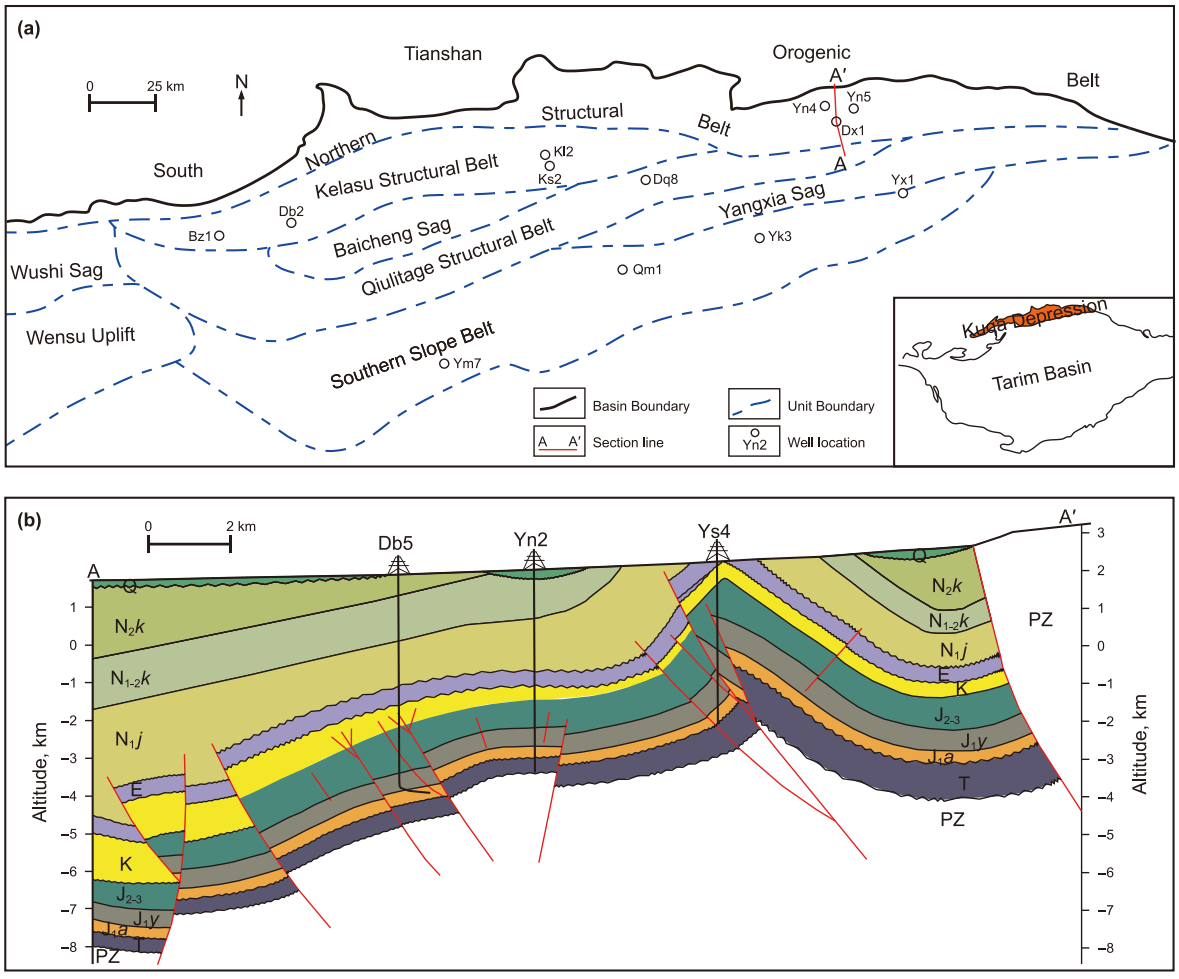

Fig. 1. Maps show the structural division of the Kuqa Depression within North Tarim Basin of West China (Li et al., 2022).

the pore bodies, and then the mercury will be extruded from the samples with decreasing injection pressure (Xi et al., 2016; Pang et al., 2024).

Conventional well logs, including calipers (CAL), Gamma Ray (GR), deep and shallow lateral logs (RD, RM), high resolution induction resistivity logs (M2R1, M2R2, M2R3, M2RX, etc), sonic transit time (DT), bulk density (DEN) and compensated neutron log (CNL), were collected. Core-to-log depth shift corrections were made to all well log curves.

Well DB101 and Well DB102 are drilled with oil based muds. Well DB5 and Well DT2 are drilled with water based muds. In addition, Well DX1, Well DB103 and Well DB104 are drilled using nitrogen drilling technology. Various types of image log data including Schlumberger's FMI (Fullbore Formation MicroImager) (Well DX1), FMI-HD (high-definition FMI) (Well DB101, DB103, DB104, DB5, DT2), Baker's EI (Earth Imager) (Well DB102) and Halliburton's XRMI (Enhanced Micro-Resistivity Imaging Tool) (Well DB103) were used to obtain the high-resolution borehole images. Static and dynamic images were generated through speed correction, centering correction and normalization, then the geological features such as fractures (natural and induced), and breakout are manually picked out, and fracture attributes and in-situ stress directions are interpreted (Nian et al., 2016). In addition, the Nuclear Magnetic Resonance (NMR) logs are processed to provide total porosity, movable fluid porosity, permeability, and other physical properties (Xin et al., 2022; Pang et al., 2022). The fundamental characterization of pore structure and reservoir quality can be continuously evaluated from continuous NMR transverse resonance time (T_2) spectra (Lai et al., 2018; Pang et al., 2024).

3.2. Theory and methods

The in-situ stress state including the magnitude and orientation, is important for oil and gas-related issues such as fluid flow, wellbore stability and fracture stimulation (Iqbal et al., 2018; Wang S. et al., 2022). The in-situ stress can be divided into three components: (1) vertical stress (S_v), (2) maximum principal horizontal stress (SH_{max}), and (3) minimum principal horizontal stress (Sh_{min}).

As gravity is directed downwards, the S_v is assumed to be vertical. The SH_{max} and Sh_{min} orientation can be determined from the induced fractures and borehole breakouts, which can be picked out from image logs (Ameen et al., 2012; Nian et al., 2016; Rajabi et al., 2016). Drilling-induced fractures, which are emerged due to the local stress field surrounding the wellbore, are parallel to SH_{max} (Wilson et al., 2015). Borehole breakouts represent enlargements of the wellbore that are triggered by in-situ stress concentrations, effectively serving as indicators of the orientations of Sh_{min} (Zoback et al., 2003; Massiot et al., 2015; Lai et al., 2024).

By constructing 1-D MEMs (one-dimensional mechanical Earth models), the magnitudes of SH_{max}, Sh_{min} and S_v can be determined (Zoback et al., 2003; Tingay et al., 2009; Lai et al., 2019). The vertical

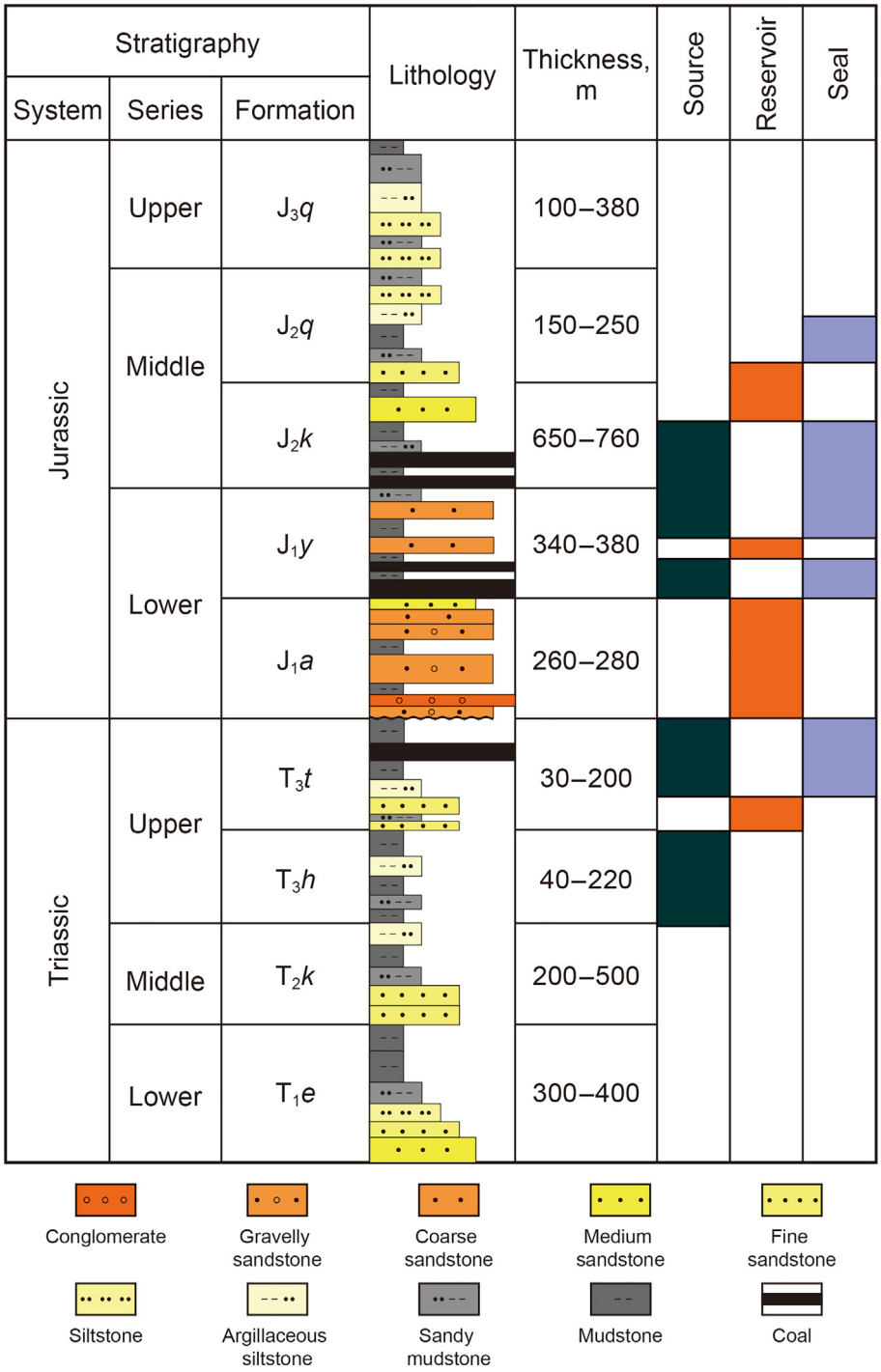

Fig. 2. Generalized Triassic-Jurassic stratigraphy and the source-reservoir-cap assemblage of Kuqa Depression (Zhang et al., 2020; Wei et al., 2022).

stress is caused by the gravity of overburden rocks (Rajabi et al., 2016). The magnitude of S_v corresponds to the weight of overburden rocks, and can be determined using Eq. (1) (Verweij et al., 2016; Lai et al., 2022).

$$S_v = \int_0^H \rho g dz \tag{1}$$

where, S_v is the vertical stress (MPa), H is the burial depth, m, ρ is the bulk density from DEN log, kg/m^3, g is the gravitational acceleration (m/s^2) (Maleki et al., 2014; Verweij et al., 2016; Ju and Wang, 2018).

Pore pressure (P_p), also referred to as formation pressure at a given depth at a certain depth (Grollimund et al., 2001; Dixit et al., 2017), can be calculated from sonic well logs by Eq. (2) proposed by Eaton (1969).

$$P_p = P_0 - (P_0 - P_w)(\Delta t_n/\Delta t)^c \tag{2}$$

where P_p is the pore pressure (MPa), P_0 is the overburden pressure

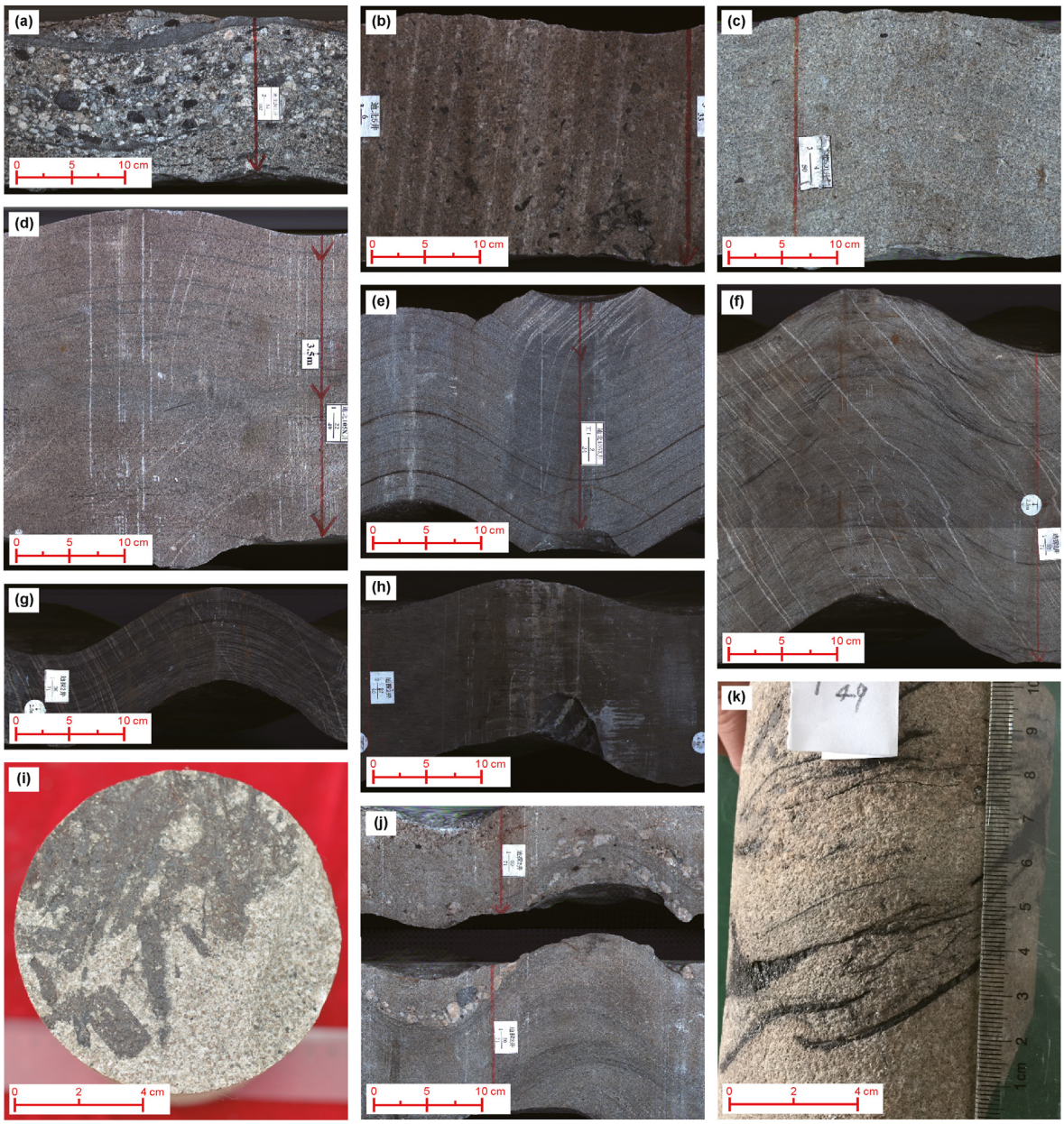

Fig. 3. Core photos showing the lithology and sedimentary structures in Jurassic Ahe Formation in Kuqa Depression
(**a**) Conglomerates with gravels arranged in a directional manner, Well DB501, 5629.78 m
(**b**) Massive gravelly sandstones, Well DB 5, 6054.17 m
(**c**) Coarse-grained sandstone, Well DB501, 5858.69 m
(**d**) Medium-grained sandstones with trough cross beddings, Well DB105X, 4763.16 m
(**e**) Fine-grained sandstones with parallel beddings, Well DB105X, 5009.43 m
(**f**) Siltstones with wavy beddings, Well DT2, 5096.65 m
(**g**) Silty mudstones with horizonal beddings, Well DT2, 5096.04 m
(**h**) Massive dark mudstones, Well DT2, 5106.03 m
(**i**) Carbonized plant fragments in sandstones, Well DB105X, 4764.17 m
(**j**) Reactivation surfaces, Well DT2, 5099.7 m
(**k**) Coal lines in sandstones, Well DB105X, 4761.43 m.

(MPa), P_w is hydrostatic pressure (commonly taken as 9.8 MPa km^{-1}), Δt_n is sonic interval transit time at normal pressure, Δt is sonic transit time. C is the coefficient of compaction (Eaton, 1969; Ju et al., 2017). It is related to the compaction of the strata. It can be obtained either through inverse calculation using measured pore pressure data or by establishing a normal compaction trend line and then performing a linear fit of the response of sonic transit time to compaction.

The determination of the Sh_{min} and SH_{max} magnitude via well logs can be calculated based on vertical stress, Poisson's ratio, and pore pressure (Eqs. (3) and (4)) (Eaton, 1969; Maleki et al., 2014; Lai et al., 2022).

$$SH_{max} = \frac{\nu}{1-\nu} S_V + \frac{1-2\nu}{1-\nu} \alpha P_p + \frac{E}{1-\nu^2} \varepsilon_H + \frac{E_v}{1-\nu^2} \varepsilon_h \quad (3)$$

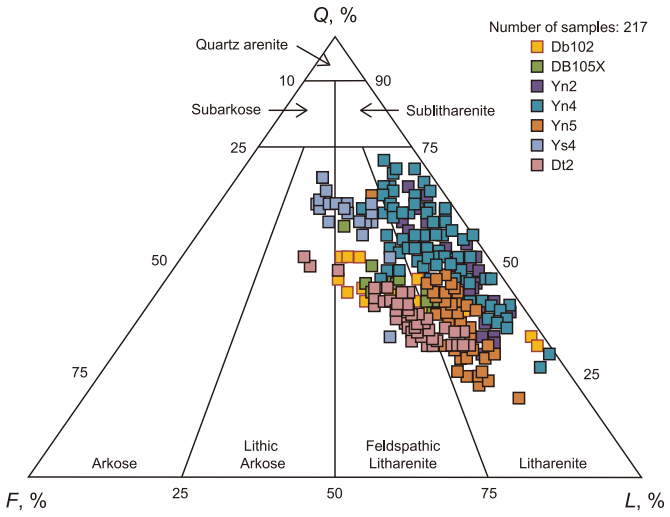

Fig. 4. Classification of sandstone using Folk's (1980) classification of Jurassic Ahe Formation in Kuqa Depression.

$$Sh_{\min} = \frac{v}{1-v}S_V + \frac{1-2v}{1-v}\alpha P_p + \frac{E}{1-v^2}\varepsilon_H + \frac{E_v}{1-v^2}\varepsilon_H \quad (4)$$

where E (GPa) is Young's modulus and v is Poisson's ratio. Coefficient α is the Biot's coefficient, which can be obtained using an empirical equation. The ε_H and ε_h are the coefficients related to the maximum and minimum horizontal stress magnitudes.

Under the background of strong tectonic compression, the formation has strong heterogeneity and anisotropy, and SH_{max} is not equal to Sh_{min}. The calculated results reveal that the in-situ stress regime belongs to the strike-slip faulting regime in which $SH_{max} > S_v > Sh_{min}$ of the Jurassic Ahe Formation in Kuqa Depression, additionally the horizontal stress difference ($\Delta\sigma = SH_{max} - Sh_{min}$) (Eq. (5)) will vary greatly due to the complexity of the structure (Maleki et al., 2014; Ju and Wang, 2018; Liu et al., 2018a).

$$\Delta\sigma = SH_{max} - Sh_{min} \quad (5)$$

where $\Delta\sigma$ is the horizontal stress difference (MPa) (Liu et al., 2018a).

4. Results

4.1. Petrological characteristics

The lithology of the Ahe formation in Kuqa Depression varies widely and the overall grain size is coarse. Core observation show that the Ahe formation is mainly composed of medium-coarse sandstone and gravelly sandstone (Fig. 3). In addition, there are thin layers of interbedded fine-grained sandstone and mudstone, while conglomerate is locally developed (Fig. 3). The sedimentary characteristics can be obviously recognized in the core observations. Carbonized plant fragments, carbon chips and coal lines indicate that the Ahe Formation is deposited in braided river delta plain sub-facies (Fig. 3). The gravels in conglomerate are arranged in a directional manner (Fig. 3(a)). The gravelly sandstone or coarse sandstone are mainly massive without visible beds (Fig. 3(b) and (c)), while the fine to medium-grained sandstones have parallel beds, oblique beds and cross beds (Fig. 3(d) and (e)). Wavy beds are detected in siltstones (Fig. 3(f)). Silty mudstones are gray to brown in color and generally exist horizontal beds (Fig. 3(g)). Meanwhile dark mudstones normally have no visible beds (Fig. 3(h)). In some cases, other sedimentary structures such as carbonized plant fragments (Fig. 3(i)), reactivation surfaces (rapid change from sandstones into conglomerates) (Fig. 3(j)) or coal lines (Fig. 3(k)) can be observed in sandstones.

The sandstones in Ahe Formation are classified mainly as litharenites and feldspathic litharenites according to Folk's classification scheme (1980) (Fig. 4). Detrital mineralogy is dominated by quartz and rock fragment, with less feldspar. The quartz ranges from 40% to 50%, with an average of 44.4%, and the average feldspar content is 11.4%, varying from 10% to 20%. The dominant feldspar is variably altered K-feldspar, with a small amount of plagioclase. The rock fragments range from 40% to 50%, with an average of 44.2%. The main types of rock fragments are metamorphic rock fragments such as silicic rocks, phyllite or quartzite, with minor amounts of volcanic and volcanic rocks. The matrix content is low (1%–25%; average 11.3%), mainly consisting of illite, mixed-layered illite/smectite and chlorite (Fig. 5(a) and (b)). Carbonate cement is the dominant cements filling the pore spaces, and the content is generally less than 1%, but can reach up to 10% in a few samples. The grain size are mainly coarse-grained, moderately to well-sorted with subrounded to subangular grain shape. The sandstones are mainly grain supported, and the grain contacts are dominantly long and concave-convex contacts, and some are point-long contacts (Fig. 5(c)). Therefore it could be concluded that the tight sandstone reservoir of the Ahe Formation are generally characterized by low compositional maturity but moderate textural maturity.

4.2. Reservoir spaces

The reservoir spaces of the Ahe Formation are mainly intragranular dissolution pores (Fig. 5(d)), intercrystalline pores in clay minerals (Fig. 5(e)) and micro-fractures (Fig. 5(f)), while residual intergranular pores, intergranular dissolution pores (Fig. 5(g)) and moldic pores (Fig. 5(h)) are occasionally observed. Intragranular dissolution pores are important reservoir spaces of the Ahe Formation, and the presence of intragranular dissolution pores is closely related to framework grains type and content (especially felspars, rock fragments), and fluid activity. Micro-fractures, which are related to tectonic movement, will not only increase the reservoir space to a certain extent, but also can effectively enhance the reservoir quality and fluid flow in tight sandstones. Generally, the feldspar and rock fragment grains with good sorting are dissolved to form intragranular dissolved pores along the micro-fractures (Fig. 5(i)). Consequently the presence of micro-fractures will enhance framework grain dissolution. In addition, although intercrystalline pores in clay minerals can act as a kind of reservoir space, their pore sizes are mostly several microns with very poor connectivity, which can be negligible for reservoir spaces.

4.3. Depositional factors contributing to reservoir quality

The depositional environment has the important control on reservoir quality by way of dictating initial sediment composition, texture and pore fluid composition (pH, Eh) (Baker, 1991; Lai et al., 2015). Different depositional environments have differences in sandstone texture (grain size and sorting) and sand composition, which control the initial intergranular volume (IGV), and additionally affect diagenetic alterations and determine reservoir quality (Taylor et al., 2010; Nguyen et al., 2013). Therefore, the depositional microfacies and lithology comprehensively reflect the depositional water energy, compositional maturity and petrological textural maturity, which are the material basis and prerequisite for the development of high-quality reservoirs (Ozkan et al., 2011).

The depositional systems of Ahe Formation are interpreted as braided river channels and overbanks microfacies in braided delta

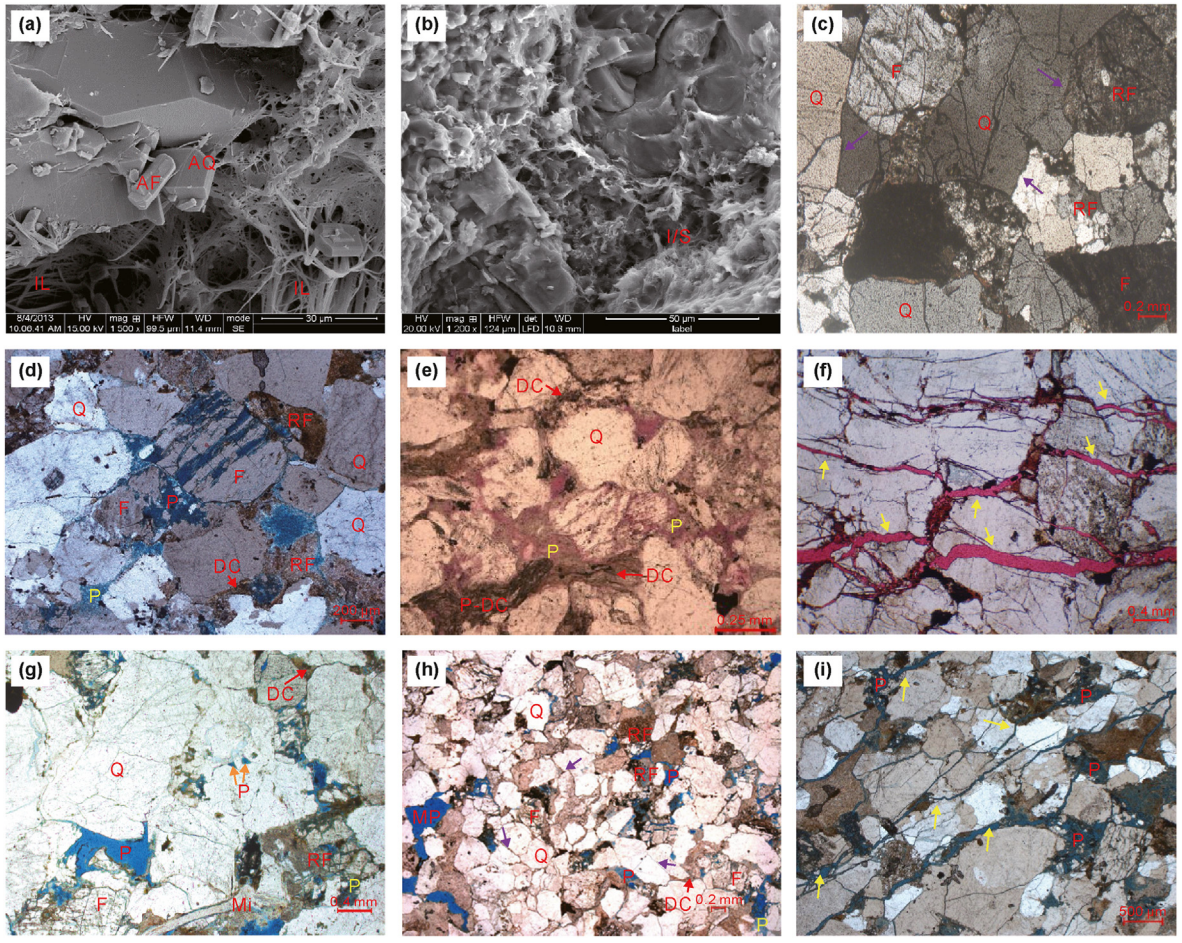

Fig. 5. Photomicrographs showing the lithology characteristics and pore systems of Ahe Formation in Kuqa Depression
(**a**) Authigenic quartz and feldspar, intercrystalline pores in illite, DB102, 4985.33 m, SEM
(**b**) Mixed layers of illite/smectite, DB105X, 4762.14 m, SEM
(**c**) Coarse-grained with gravels, long and concave-convex contact (purple arrow), moderate sorting, subangular, Well DB5, 6048.23 m, XPL
(**d**) Abundant intragranular pores due to grain dissolution, DB5, 5838.15 m, PPL
(**e**) Abundance of intercrystalline pores (P) in clay minerals, phyllite rock fragments seen as false matrix, Well DB102, 4936.85 m, PPL
(**f**) Micro-fractures (yellow arrows) with varied apertures, YN4, 4605.7 m, PPL
(**g**) Residual intergranular pores and intergranular dissolution pores, DT2, 5123.39 m, PPL
(**h**) Feldspars or rock fragments were totally dissolved forming moldic pore, DB105X, 4763.43 m, PPL
(**i**) Abundance of intragranular dissolution pores is connected by micro-fractures (yellow arrow), DB5, 5846.31 m, PPL
Q = quartz, F = feldspar, RF = rock fragments, AQ = authigenic quartz, AF = authigenic feldspar, IL = illite, I/S = mixed-layered illite/smectite, Mi = mica, DC = detrital clay, MP = moldic pores, P = pores, PPL = plane polarised light, XPL = cross polarized light. Thin sections (**d**,**g**,**h**,**i**) were impregnated with blue-dye resin, and the pores and micro-fractures are shown in blue. Thin sections (**e**,**f**) were impregnated with red-dye resin, and the pores and microfractures are shown in red.

front. Generally, braided river channel microfacies, having a bell-shaped or box-shaped GR curve shape (Fig. 6), are deposited in a high sedimentary hydrodynamics, resulting in relatively clay-free sandstone with well sorted textures and quartz- and feldspar-rich framework composition. Therefore, it is conducive for pore preservation and subsequent framework grain dissolution, and would suggest a better reservoir quality. The existence of micro-fractures in high depositional-energy sandstones can significantly enhance permeability (Fig. 6). As can be observed from core-measured porosity and permeability, the braided river channel microfacies have favorable reservoir quality (Fig. 6).

Nevertheless, overbank microfacies in the braided delta front, having high and serrated GR values (low depositional-energy, finer-grained, matrix-support) will easily experience a high compaction degree and thus a significant porosity loss (Fig. 7). In addition, clay minerals can easily block fluid migration channels, which is not beneficial for subsequent framework grain dissolution. Thus, overbank microfacies result in low porosity and tiny pore radii and poor pore structure (Henares et al., 2014) (Fig. 7). The low core-measured porosity and permeability values confirm the poor reservoir quality of overbank microfacies (Fig. 7).

To perform statistical analysis on different grain size in the braided river channel microfacies, Well YN2, which are located at the core of the fault nose and Well DT2 at the wing of the fault nose are used to analyze the reservoir quality variations of various depositional microfacies. Statistics show that the porosity of the tight sandstones in Ahe Formation increases with increasing grain sizes, as shown in Fig. 8. Among them, the porosity and permeability of conglomerates, gravelly sandstones and coarse sandstones are better. As the grain sizes become finer, the porosity and permeability in medium-fine sandstone decreases significantly (Fig. 8).

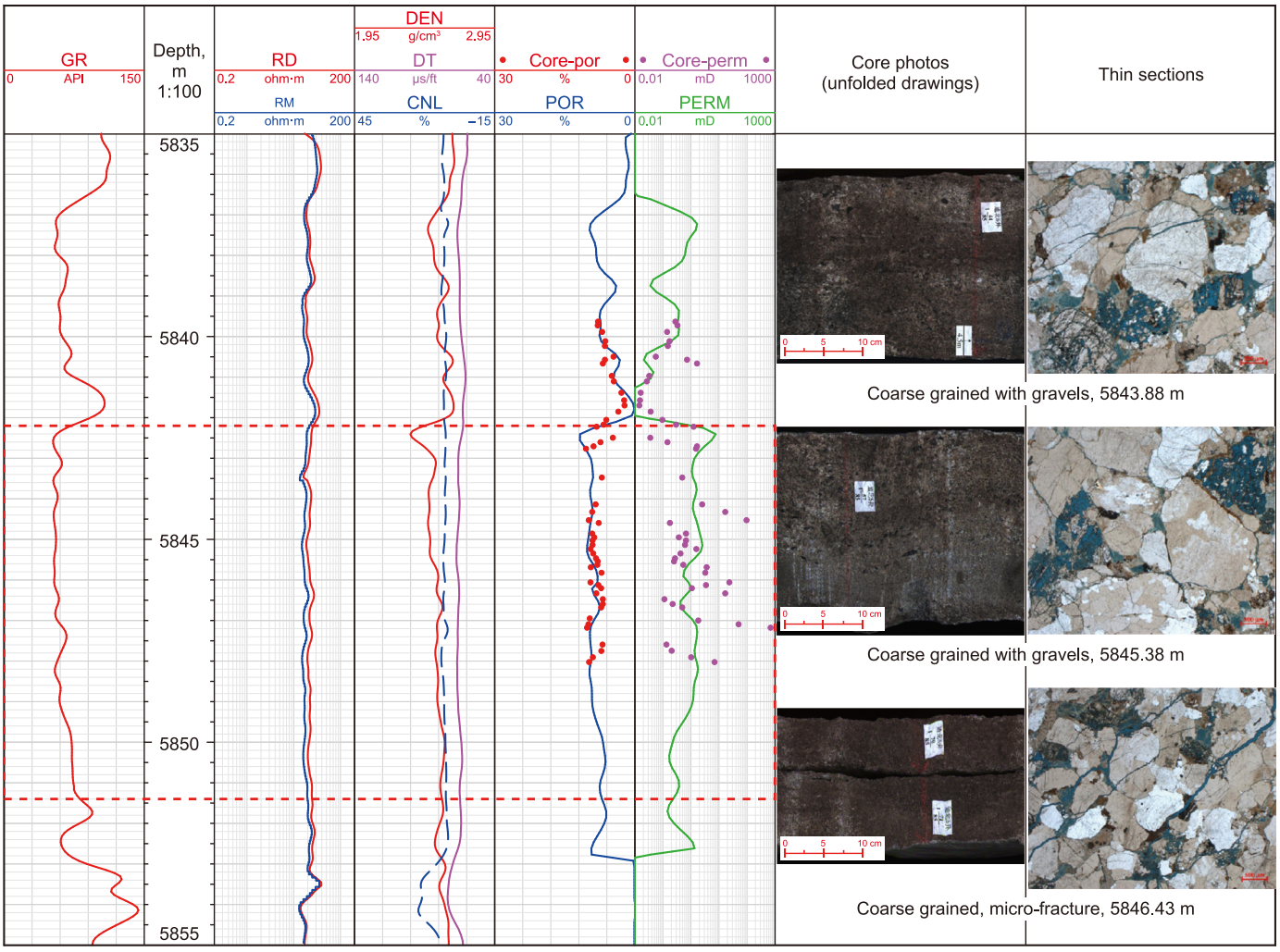

Fig. 6. Braided river channel with high depositional-energy of the Jurassic Ahe Formation in Well DB5 in Kuqa Depression.

From the sedimentary aspect, the high reservoir quality of tight sandstones in Ahe Formation is mainly found in high-energy sandstones, which have relatively coarser grained sandstones and contain minor detrital clay. The low hydrodynamic depositional environment has finer grain size and high ductile rock fragment content, and is easily compacted to form poor reservoir quality.

4.4. Diagenetic factors and reservoir quality

The analysis of thin section, cathodoluminescence and scanning electron microscope shows that the Ahe Formation has undergone destructive diagenesis such as compaction and cementation, as well as constructive diagenesis such as dissolution and fracturing, during the long geological history. Calcite, quartz and authigenic clay minerals such as kaolinite, illite, mixed layer illite/smectite and chlorite were formed in these diagenetic processes.

Compaction is one of the dominant factors that cause the deterioration of physical properties in the reservoirs. Due to the strong horizontal tectonic compression suffered by the reservoir during the late Himalayan movement, the compaction of the Ahe Formation involves vertical compaction as well as lateral (horizontal) tectonic compaction (Shi et al., 2020; Wang et al., 2020). The compaction is intense, and the grain contacts are mainly long contacts and even concave-convex contacts (Fig. 5(c)), and the mechanical compaction will result in the deformation of ductile grains such as rock fragments and micas (Fig. 9(a)). Compaction can be inhibited by early carbonate cements (Dutton and Loucks, 2010; Higgs et al., 2017). However, due to the overlying Yangxia Formation and Kezilenuer Formation coal-bearing strata, the stratigraphic water in the early diagenesis stage was acidic, which inhibited the formation of carbonate cements, making the rocks more prone to compaction. This is also an important factor that makes it difficult to preserve primary intergranular pores in the Ahe Formation.

At the same time, acidic fluids formed by organic matter decarboxylation promote the dissolution of feldspars and rock fragments in the reservoir (Fig. 9(b) and (g)), playing an important role in improving physical properties. Generally, the dissolution of rock fragments is weaker than that of feldspar. The matrix is the weakest and can only form micro-pores (Fig. 5(f)). The cementation strength of the Ahe Formation is weak as a whole, and the cement is only enriched locally. Three different cementation types are recognized: (1) Quartz cementation, mainly in the form of quartz overgrowth (Fig. 9(c)); (2) Carbonate cementation. Mosaic-type textures are the most common texture (Fig. 9(d)), although locally pervasive cementation has been recognized (Fig. 9(e)). (3) Authigenic clay minerals, which occur in the form of pore filling and pore bridging (Fig. 9(h) and (i)). The considerable amounts of micropores in the tight sandstones are attributed mainly to the

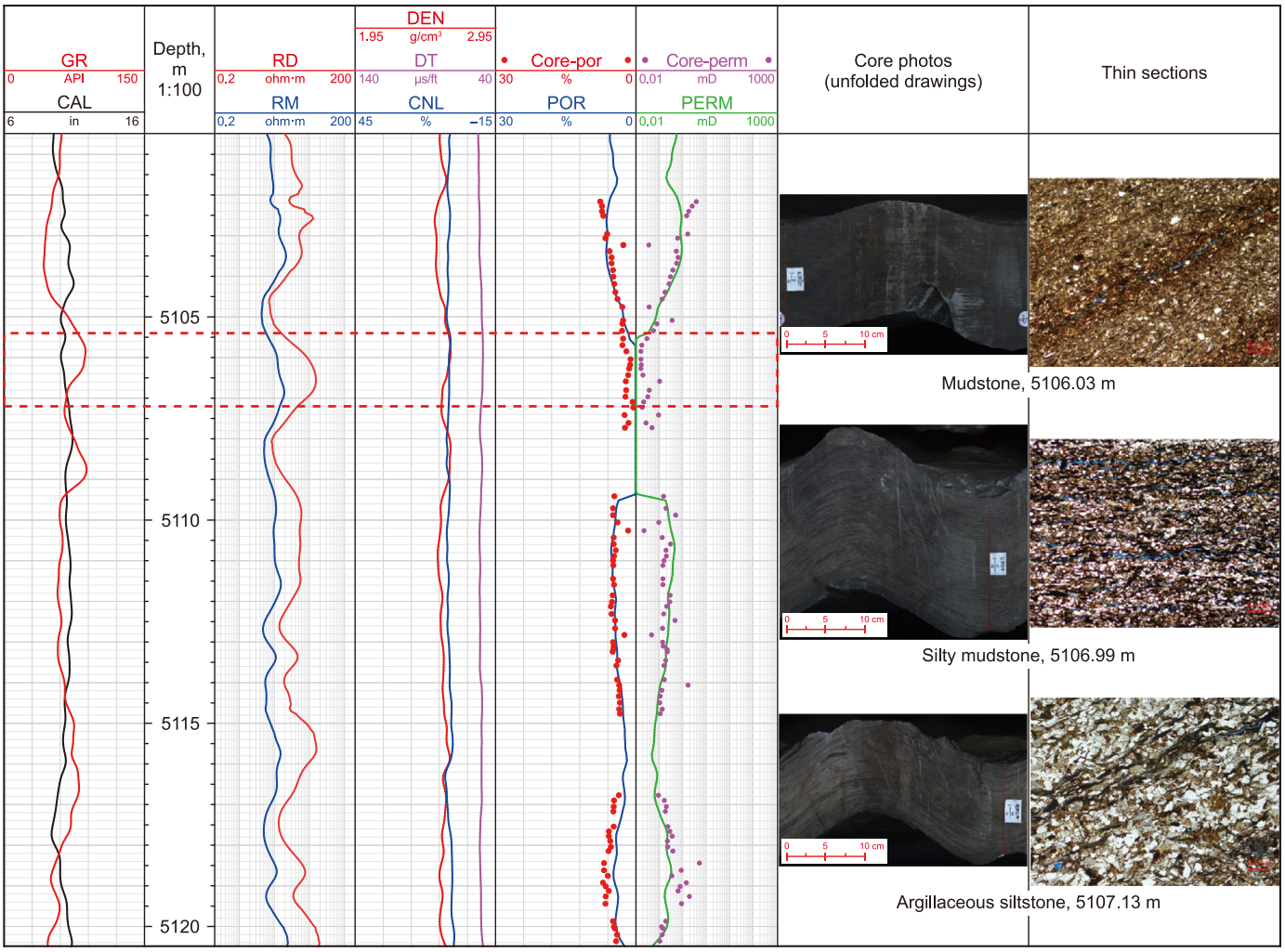

Fig. 7. Overbank with low depositional-energy of the Ahe Formation in Well DT2 in Kuqa Depression.

presence of clay minerals (Salem et al., 2005; Dutton and Loucks, 2010; Cui et al., 2017).

Fracturing is formed by the tectonic compression breaking through the rock's rupture strength, which belongs to structural diagenesis. Fracturing creates micro-fractures with various apertures in the rock, which effectively communicate with fluid in the pore space, promoting dissolution and inhibiting cementation (Figs. 5(i) and 9(f)). The common phenomenon of dissolution along the fractures can be observed. Although the storage capacity of micro-fractures is limited, they can form a network system that connects the matrix pores, effectively improving the seepage capacity of the reservoir and significantly improving reservoirs' physical properties.

Only considering diagenetic factor, various diagenesis types and diagenetic minerals play a very important role in pore systems and reservoir properties. As shown in Fig. 10, reservoirs with higher porosities are mainly associated with a high abundance of dissolution pores (Fig. 10(a)), and reservoirs with lower porosities are mainly related to high carbonate cement and high clay mineral content (Fig. 10(b and c)). In other words, dissolution is an important contributor to porosity enhancement, and the dissolution porosity is demonstrated by the occurrence of honeycombed pores and partial dissolution of feldspar and rock fragment grains (Figs. 9(b) and 11(a)). Micro-fractures formed by fracturing can promote fluid flow, and enhance dissolution, and significantly improve the permeability of reservoirs (Figs. 9(f) and 11(b–c)). Local interval (mainly mud-sand boundaries) is cemented by carbonate cement, and the sandstones tightly cemented with carbonates have the lowest thin section porosity and poor reservoir quality (Fig. 11(d)). With the increase of clay mineral content, porosity and permeability of sandstones decrease, and the pore structures deteriorate (Fig. 10(c)). It can be seen in thin section that clay minerals fill the pores in the form of pore filling and pore bridging and micropores dominate the pore systems (Fig. 11(e)). Meanwhile due to lack of the rigid grains, the lowest quality reservoirs are mainly associated with intervals rich in detrital clays or ductile rock fragments, or those very fine grained or very poorly sorted successions, which are easily compacted (Figs. 7 and 11(f)).

4.5. Tectonic factors (fracture and in-situ stress)

Adjacent to the South Tianshan orogenic belt, the study area has been in a strong compressional tectonic setting for a long time. Tectonic activity is an important factor leading to the difference of reservoir physical properties. However, the impact of tectonics on the reservoir is dual. On the one hand, strong compression will cause compaction and pore reduction; on the other hand, brittle sandstones exceed the rupture strength of the rocks, forming

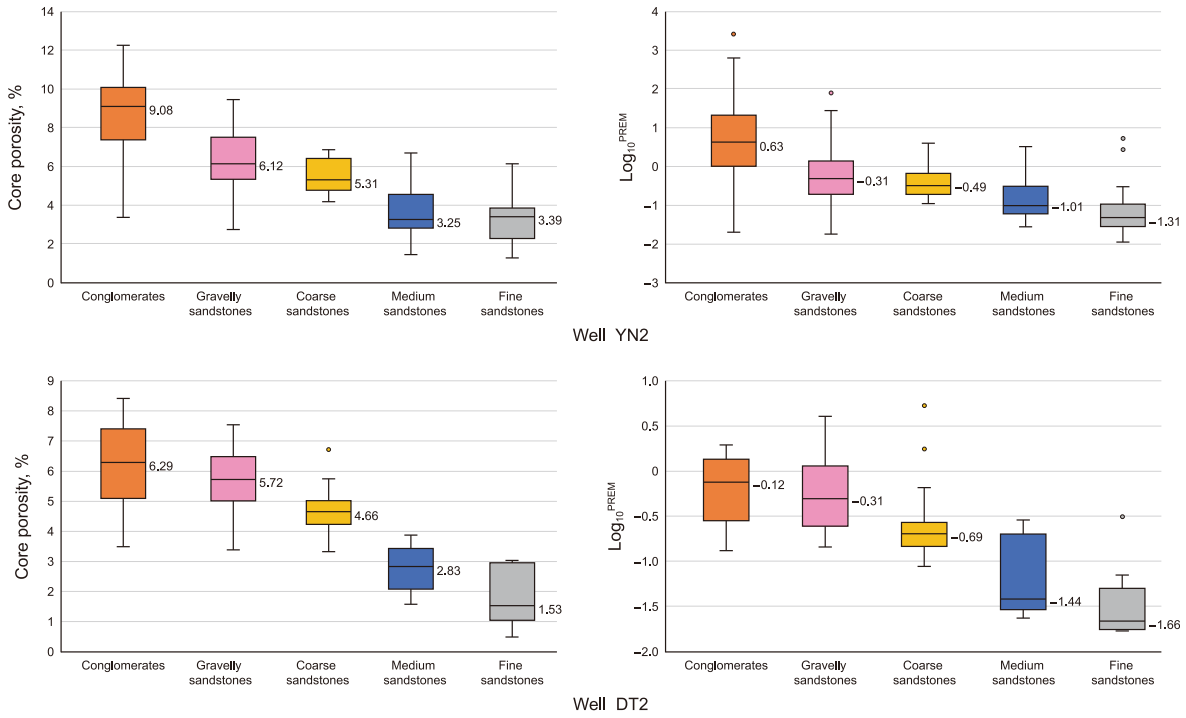

Fig. 8. The box plot shows the differences in porosity and permeability of five types of lithologies of Jurassic Ahe Formation in Well YN2 and Well DT2 in Kuqa Depression.

macro-microscopic fractures and increasing the heterogeneity of the reservoir (Zhang et al., 2021). The in-situ stress refers to the internal stress within the Earth's crust, which is linked to both gravitational and tectonic forces (Ju and Wang, 2018). It can effectively characterize the impact of tectonic activity on the reservoir. The present in-situ stress is the inheritance and development of paleo-tectonic stress. Therefore, the in-situ stress state, which include the magnitude or orientation (Grollimund et al., 2001), play a vital role in fracture stimulation, reservoir evaluation, fluid flow (Tingay et al., 2009; Liu et al., 2018b).

The in-situ stress can be divided into vertical stress (S_v), maximum principal horizontal stress (SH_{max}) and minimum principal horizontal stress (Sh_{min}). The magnitude and orientation can be distinguished and calculated by image logs and array acoustic logs. The horizontal stress difference ($\Delta\sigma$) can effectively reflect the degree of lateral compression caused by tectonics. The study shows that the in-situ stress has obvious control over the matrix physical properties and fracture effectiveness of the reservoirs.

4.5.1. In-situ stress and matrix physical properties

The horizontal stress difference ($\Delta\sigma$) plays an important role in matrix physical properties and pore structure. The crossplot in Fig. 12 shows that there is a significant negative correlation between matrix porosity and horizontal stress difference ($\Delta\sigma$). With the increase of the horizontal stress difference, the microscopic pore structure becomes complex, and the macroscopic reservoir quality becomes worse. Under the same in-situ stress condition, the finer grained size or the worse sorting, the weaker the compaction resistance and the denser the physical properties (Fig. 13(a) and (c)).

The depth of about 5841.1 m (GR = 84.2 API) in Fig. 13(b) is characterized by a relatively high $\Delta\sigma$ value, and the sandstones are fine-grained, and rich in detrital clays, experienced a very high degree of compaction as revealed by the thin section. No obvious pores can be seen, and the T_2 distributions are narrow. The pore distribution plot also visually reflects these same characteristics, with a larger column area representing micropores on the left and almost no column area representing macropores. So, high $\Delta\sigma$ value indicate poor pore structure and reservoir quality. The depth of about 5844.1 m has a relatively moderate $\Delta\sigma$ value (Fig. 13(c)), and the sandstones, coarse-grained, well sorted, have a better resistance to compaction. The thin section can be seen the increase of intragranular dissolution pores. The T_2 distributions and pore distribution plot also visually reflect these same features. Compared with Fig. 13(b), the T_2 spectrum exhibits significant broadening and the value of the right peak increases significantly while the value of the left peak decreases in pore distribution plot. However, if the sandstones are poorly sorted or are abundant in soft grains such as micas or rock fragments, the degree of compaction will also be high even with a moderate $\Delta\sigma$ value (Fig. 13(a)). The depth of about 5847.1 m in Fig. 13(d) is characterized by obvious low $\Delta\sigma$ value. With the appearance of microfractures, the sandstones experienced a very high degree of dissolution. Correspondingly, NMR logging shows that this depth interval has high reservoir physical properties, wide T_2 distributions, and contain tail T_2 distributions. The pore distribution plot also visually reflects these same features, with a larger column area on the right side representing the macropores (Fig. 13(d)). Thus, low $\Delta\sigma$ value indicate the high reservoir quality.

4.5.2. In-situ stress and fracture effectiveness

In addition to matrix pores, fractures are important factors for improving reservoir permeability and hydrocarbon productivity. Fractures of various scales are able to connect isolated pores, enhancing pore connectivity, and improving overall permeability (Boutt et al., 2009). As the migration channel of fluids, fractures are also the key factors affecting the dissolution of tight reservoirs (Baqués et al., 2020). The two intuitive factors that affect fracture effectiveness are the degree of fracture filling and the fracture opening controlled by the stress field. Core photos show that the fracture surfaces of different lithologies in the Ahe Formation have obvious scratches and no obvious filling (Fig. 14). Therefore, the

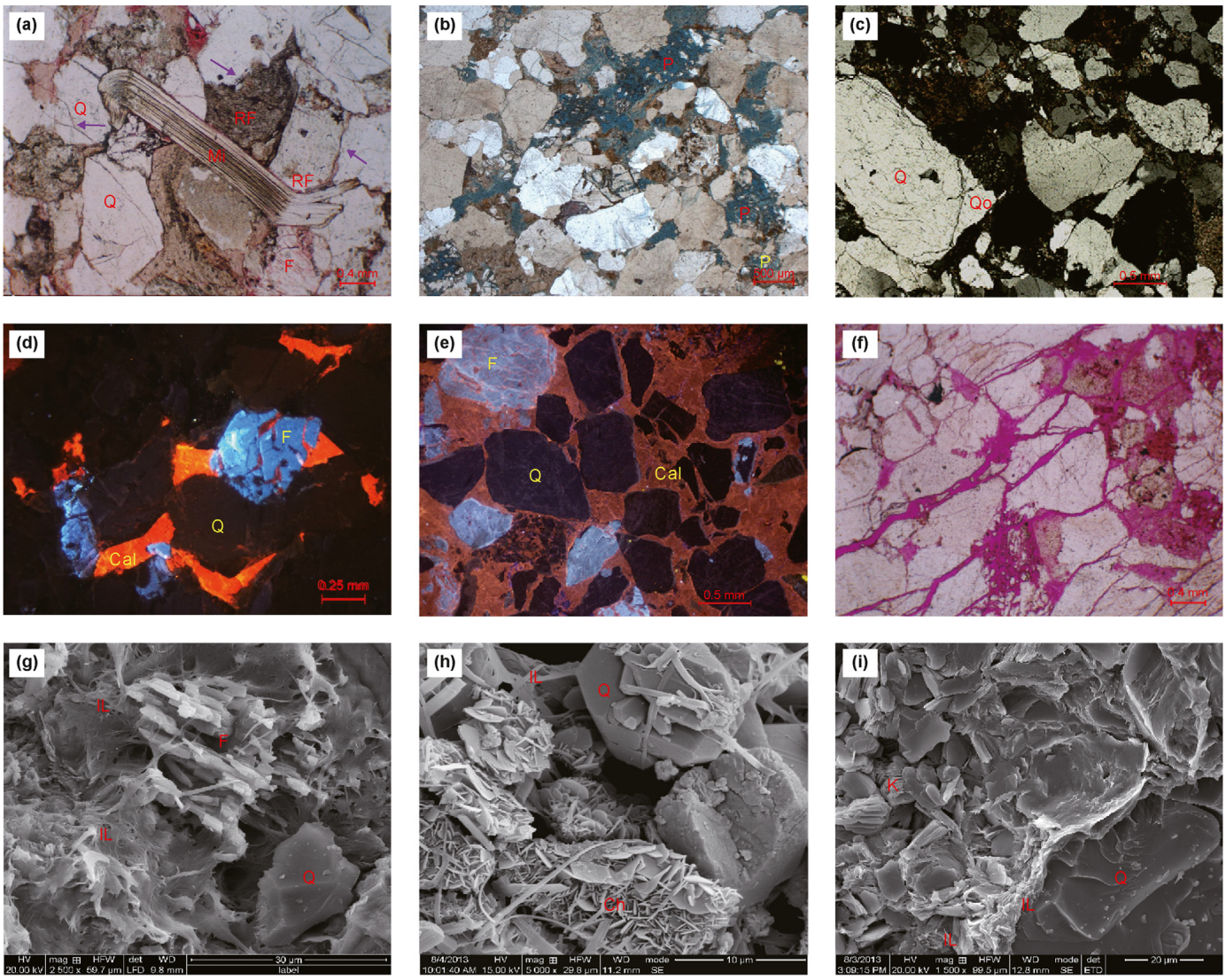

Fig. 9. Photomicrographs showing the microscopic diagenetic features of Jurassic Ahe Formation in Kuqa Depression
(**a**) Compaction, long and concave-convex contact, deformation of mica, rupture of quartz particles, Well YN2, 4730.4 m, PPL
(**b**) Dissolution, dissolution of feldspar, rock fragment and matrix, Well DB5, 5844.83 m, PPL
(**c**) Cementation, euhedral overgrowth of quartz, DB102, 4986.36 m, XPL
(**d**) Cementation, mosaic-type textures in calcite cements, DB102, 5096.06 m, CL
(**e**) Cementation, pervasive cementation of carbonate, DB102, 4942.62 m, CL
(**f**) Fracturing, micro-fractures with varied apertures, dissolution along the fracture planes, YN5, 4773.28 m, PPL
(**g**) Dissolution of feldspar along its cleavage, and pore-lining illite displays fibrous and hair-like crystals, DB105X, 4772.73 m, SEM
(**h**) Authigenic clay minerals, willow chlorite attached to particle surface, DB102, 4985.33 m, SEM
(**i**) Authigenic clay minerals, vermicular kaolinite and flake illite, which occur in the form of pore filling and pore bridging, DB102, 4937.82 m, SEM
Q = quartz, F = feldspar, RF = rock fragments, Qo = quartz overgrowth, Mi = mica, Cal = calcite, Ch = chlorite, IL = illite, K = kaolinite, P = pores, PPL = plane polarised light, XPL = cross polarized light, CL = Cathodoluminescence. Thin sections (**a**,**f**) were impregnated with red-dye resin, and the pores and microfractures are shown in red. Thin section (**b**) were impregnated with blue-dye resin, and the pores and microfractures are shown in blue.

stress field in the study area is the main controlling factor for fracture effectiveness.

Both the orientation and magnitudes of the in-situ stress field affect the presence and attributes (fracture aperture) of fractures. The generation of natural fractures is often influenced by paleo-stress, whereas the in-situ stress primarily governs fracture permeability and aperture (Zeng et al., 2010; Liu et al., 2018b; Lai et al., 2019). Fractures may vary in their effectiveness according to in-situ stress conditions. Fractures strike parallels to the orientations of the current maximum horizontal principal stress (SH_{max}) exhibit the smallest normal stress on their surfaces, leading to a tendency towards larger apertures and better effectiveness. When fractures strike is perpendicular to the current SH_{max}, the planes have the largest normal stress on their surfaces, tending to be small in aperture and poor in effectiveness. Effective natural fractures can release stress, and corresponding layers show low values of $\Delta\sigma$. However, in areas where fractures are not developed or closed, the in-situ stress is relatively concentrated and at a high $\Delta\sigma$ value.

The rose diagram in Well DB102 shows that the natural fracture orientation is mainly 75°–255°. The borehole breakout direction indicates the direction of the minimum horizontal principal stress, which is 70°–250°. In addition, the in-situ stress field is strong and

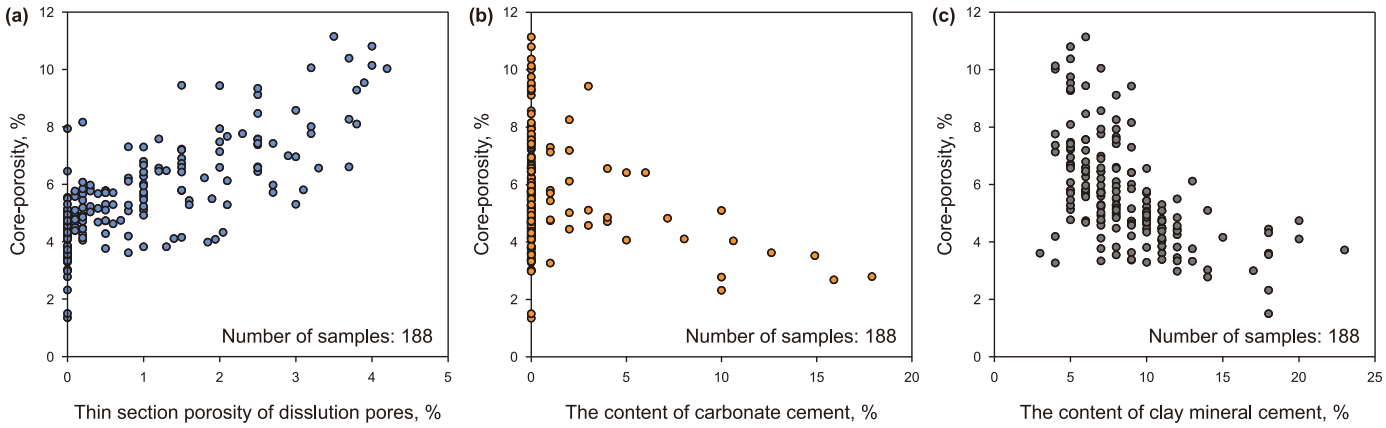

Fig. 10. The relationship between the core-porosity and the thin section dissolution porosity, the carbonate cement content, the clay mineral cement, respectively of Jurassic Ahe Formation in Kuqa Depression.

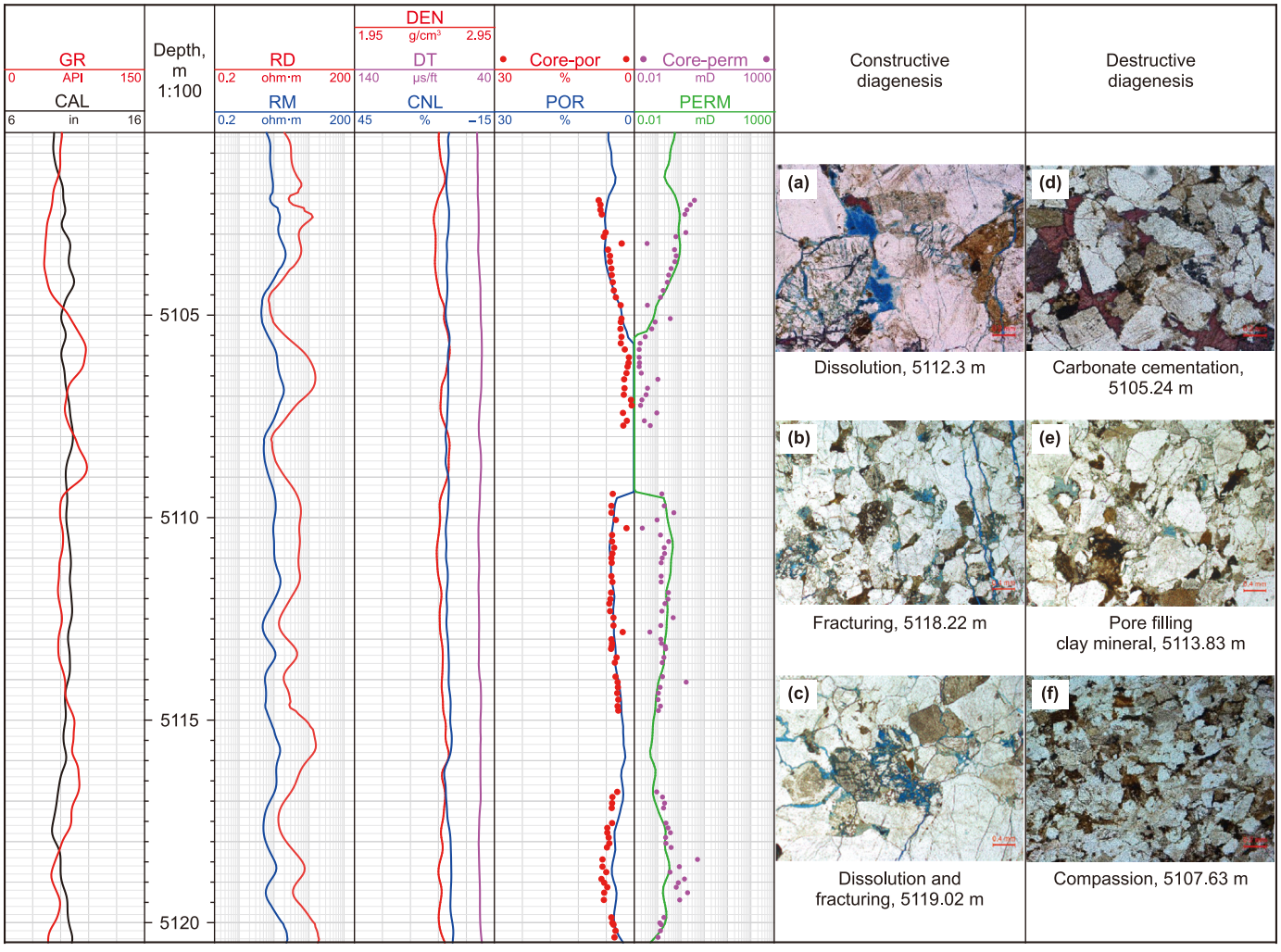

Fig. 11. The relationship between the physical properties and the diagenesis of Jurassic Ahe Formation in Kuqa Depression.

the value of $\Delta\sigma$ is relatively high. The histogram shows that $\Delta\sigma$ value is concentrated between 25 and 40 MPa, with an average value of 31.9 MPa. The fracture orientation is perpendicular to the maximum principal stress direction, and the stress on the fracture surface is large, resulting in poor effectiveness (Fig. 15). The conclusion is confirmed from the side that there is little difference in $\Delta\sigma$ value between the intervals with fractures and sandstones without fractures. Conversely, the rose diagram shows that the strike of natural fracture is mainly 65°–245° in Well DX1. The rose diagram of borehole breakout reveals that the Sh_{min} orientation is

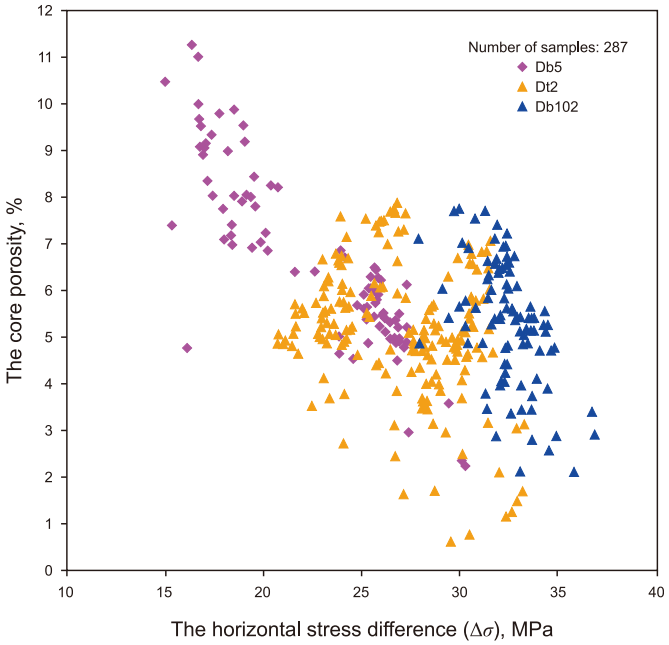

Fig. 12. Cross plot of the core porosity versus the horizontal stress difference of Jurassic Ahe Formation in Kuqa Depression.

close to 130°–310°. The induced fractures indicate the SH_{max} direction, which is approximately 40°–220°. The average $\Delta\sigma$ value is 24.6 MPa, with a range of 15–35 MPa. Natural fractures in this stress state are suggested to exhibit open state and good connectedness since the intersection angles between SH_{max} orientation and fractures strike are within 30° and the normal stress on the fracture surfaces is small (Fig. 16).

As illustrated in Fig. 16, the intervals with effective fractures are corresponding to the low $\Delta\sigma$. The $\Delta\sigma$ is the lowest in depth of about 4821 m, and multiple oblique fractures and one high-angle straight fracture can be observed in image logs (Fig. 16(a)). For fractures with the same strikes, the normal stress on the high-angle fracture surface is smaller than that on the low-angle or horizontal fracture surface, so high-angle fractures could have greater apertures and greater effectiveness and the $\Delta\sigma$ value is the lowest (Lai et al., 2019; Zeng et al., 2023). The high $\Delta\sigma$ layers are either fractures with poor effectivity or sandstones without fractures (Fig. 16(c)).

In summary, the in-situ stress (orientation and magnitudes) plays an important role in controlling reservoir quality.

5. Discussion

5.1. Control of sedimentation, diagenesis, and tectonics on reservoirs quality

5.1.1. Sedimentation-diagenesis controlling matrix pores

The Dibei structural belt in North Kuqa Depression has long been under strong compressive setting, and the formation of the reservoir is jointly controlled by sedimentation, diagenesis and tectonics. The matrix pores of the reservoirs are mainly controlled by sedimentary and diagenetic factors. The sedimentary environment determines the texture and composition of the sediments. These initial differences not only control the initial intergranular volume, but also affect the diagenetic evolution, subsequently affecting the macroscopic physical properties and microscopic pore structure of the reservoir (Rezaee and Lemon, 1996; Bjørlykke, 2014). As shown in Fig. 8, in the same well, porosity increase with the increase of average grain size, which can directly show the control of sedimentation on the reservoir. Higher depositional-energy results in coarser grain size, better sorting, and superior reservoir physical properties.

Fig. 17 illustrates the vertical variation of reservoir quality under the control of sedimentation and diagenesis. In the 4934–4944.5 m depth interval of Well DB102, the *GR* curve mainly display a bell-shape, representing a typical braided river channel's depositional microfacies with positive grain sequence. The lithologies gradually change from conglomerate to medium-fine sandstone to mudstone, which represent a gradual transition of depositional energy from high to low. The thin section shows the diagenesis under the initial difference of sedimentation. Gravelly sandstone and coarse sandstone lying in the middle of braided river channel have high rigid grain content, which have a better resistance to compaction, and are conducive to pore preservation and subsequent dissolution. From the aspect of thin section, it is found that intergranular and intragranular dissolution pores are common. As the grain size becomes finer and the depositional-energy decreases, there is an increase of soft ductile minerals. Soft ductile minerals can promote compaction, meanwhile, some authigenic clay minerals fill pores to form micropores. Thin section observations reveal that the pore structure deteriorates and matrix physical properties decreases. In matrix-rich sediments, compaction is more severe (Ramm, 2000; Feng et al., 2024). Fine sandstone and argillaceous siltstone lying in the top of braided river channel are very tight with the lowest porosity. No evident pores exist in thin section observations and the reservoir quality is the poorest. In addition, although sandstones at the bottom of braided river channel are relatively coarser grained and well sorted, they also have relatively low porosities and poor reservoir quality because of carbonate cementation (Fig. 17).

In summary, changes in depositional energy have formed sandstones with varying lithology. Due to differences in detrital mineralogy, such as clay content, grain size and sorting, different intervals of the sandbodies may be modified by different diagenesis, affecting matrix pores. The superposition of high-energy sedimentary background and constructive diagenesis is conducive to the presence of matrix pores. Low-energy sedimentary background or destructive diagenesis leads to rare matrix pores and poor reservoir property.

5.1.2. Fractures and in-situ stress controlling permeability and productivity

Fractures can form a network system that connects the matrix pores, effectively improving the permeability and productivity of reservoirs. The differential distribution of in-situ stress indicates the degrees of natural fracture development and controls the effectiveness of fractures. Two wells including DB5 and DT2 in Fig. 18 are presented to unravel the controls of fractures and in-situ stress on permeability and productivity. These two wells have a similar sedimentary background, differences in the degree of fracture development and in-situ stress field distribution caused by tectonic effects result in significant variations in reservoir quality and productivity. As shown in Well DB5 (Fig. 18(a)), the high-quality reservoirs exhibit low $\Delta\sigma$ value (average 24.9 MPa). Image log fracture observations show that fractures are abundant in Well DB5, and natural fractures are approximately parallel to SH_{max} as documented on the strike composite rose diagram, indicating greater fracture effectiveness. Fractures can connect isolated pores, constitute fluid flow pathways and significantly improve permeability and hydrocarbon productivity (Ameen et al., 2012; Peacock et al., 2016). Thin sections show that effective fractures are conducive to fluid flow, and dissolution can commonly be observed

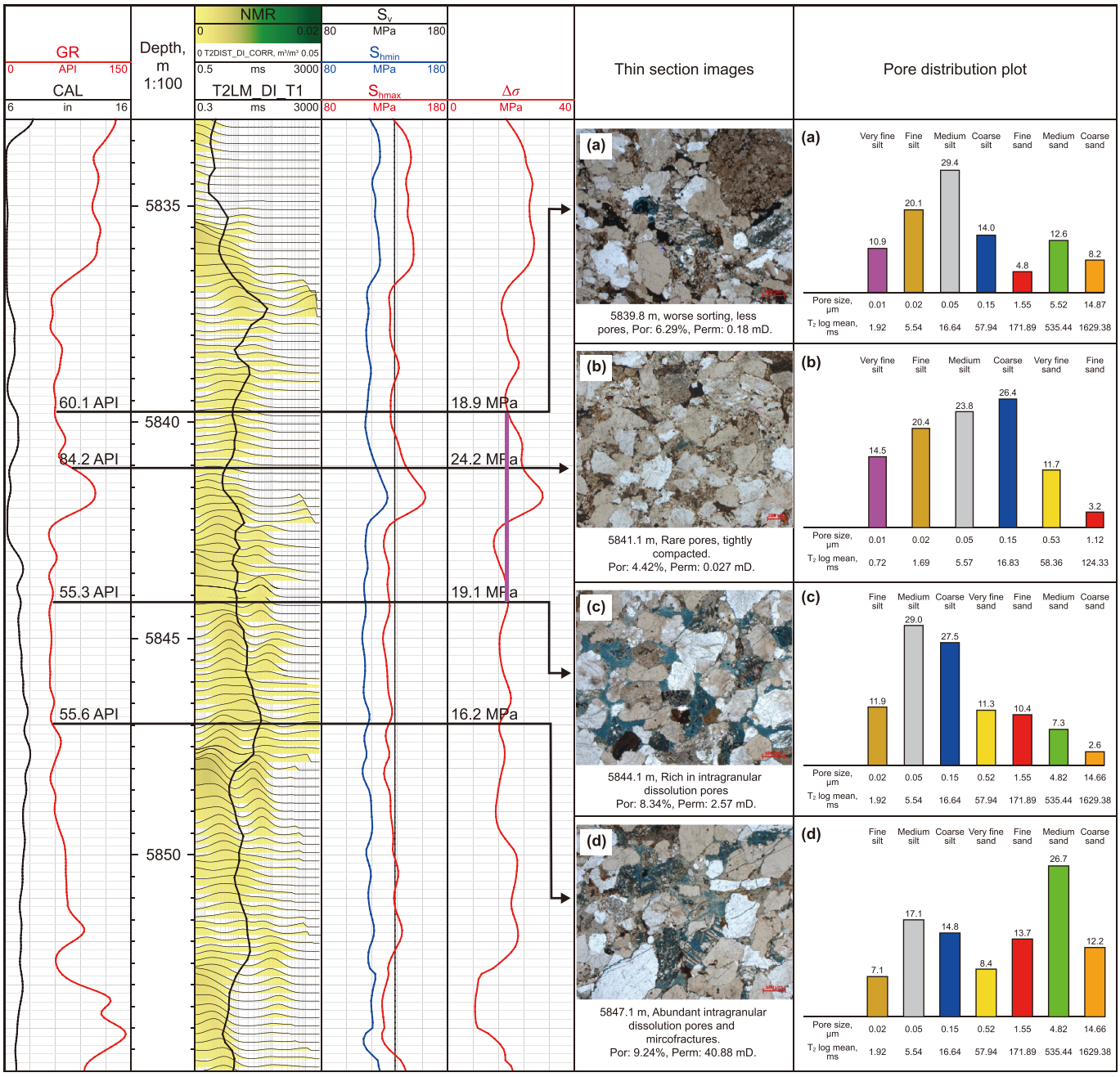

Fig. 13. In situ stress magnitude determination via well logs and related thin sections in Well DB5 of Jurassic Ahe Formation in Kuqa Depression.

along fractures. Additionally a lower threshold pressure also indicates a good pore connectivity and high permeability with larger pore spaces by MICP analysis (*Por* = 7.6 %, *Perm* = 5.62 mD, *Pd* = 0.38 MPa, r_{max} = 1.97 μm) (Fig. 18(a)). Accordingly, Well DB5 has obtained high oil and gas productivity. The oil test reveals that in the 5883.5–5925.5 m depth interval of DB5, the daily oil production is 3.36 m^3, and the daily natural gas production is 90517 m^3 with 4 mm choke width and drawdown pressure of 56.10 MPa (Table 1).

On the contrary, poor reservoirs show high Δσ values (average of 30.1 MPa) with few fractures observed in image logs and cores in Well DT2 (Fig. 18(b)). Closed fractures have strike divergence of near 70° with respect to SH_{max}. Fractures' surfaces bear larger normal stress, therefore they would tend to be small in aperture and poor in effectiveness. In the thin section view, the compaction is intense, manifesting long contacts even concave-convex contacts, and pores are isolated distribution with poor connectivity. The microscopic pore structure parameters (*Por* = 5.5%, *Perm* = 0.62 mD, *Pd* = 0.62 MPa, r_{max} = 1.21 μm) indicate the dominance of small pore throats (Fig. 18(b)). Compared with Well DB5, the permeability decreases exponentially. Therefore, it can be concluded that Well DT2 has low reservoir quality and low hydrocarbon productivity. In the 5039.5–5839.5 m depth interval of Well DT2, the oil test reveals that only 1803 m^3 daily natural gas productivity is obtained with 7 mm choke width and drawdown pressure of 5.58 MPa (Table .1).

Drawing on and citing relevant achievements of Tarim Oilfield Company, the statistical study of the relationship between fractures, in-situ stress, and hydrocarbon productivity in multiple wells

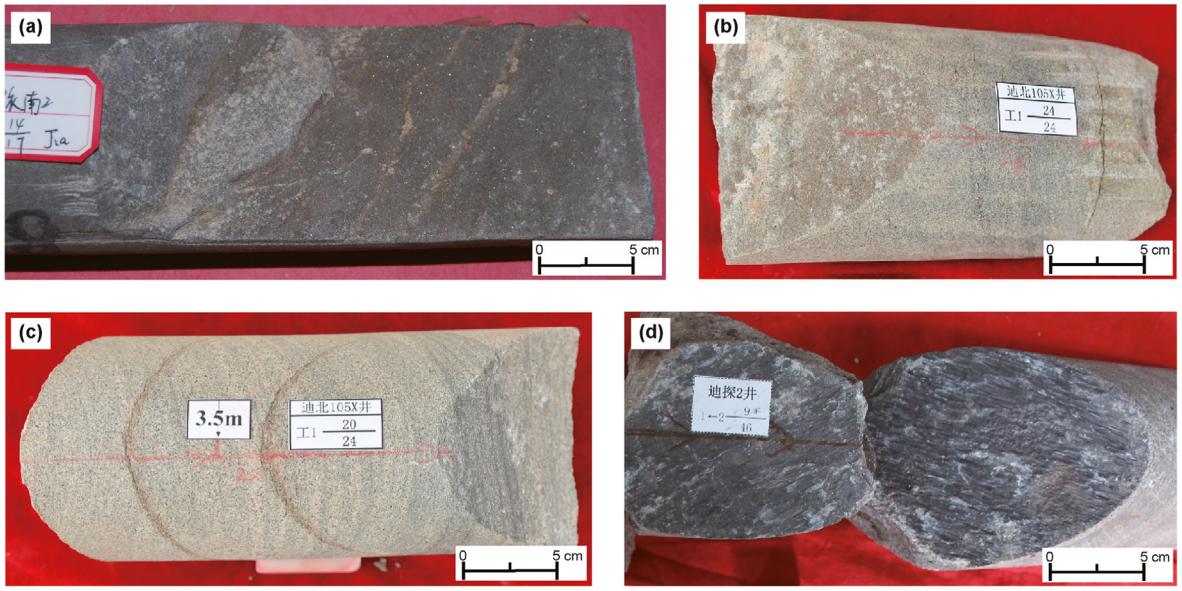

Fig. 14. Fractures in cores of the Jurassic Ahe Formation in Kuqa Depression
(**a**) Vertical fracture with no cement, Well YN2
(**b**) High angle fracture with no cement, Well DB105X
(**c**) Multiple high angle fracture, Well DB105X
(**d**) Fracture surface with obvious scratches, Well DT2.

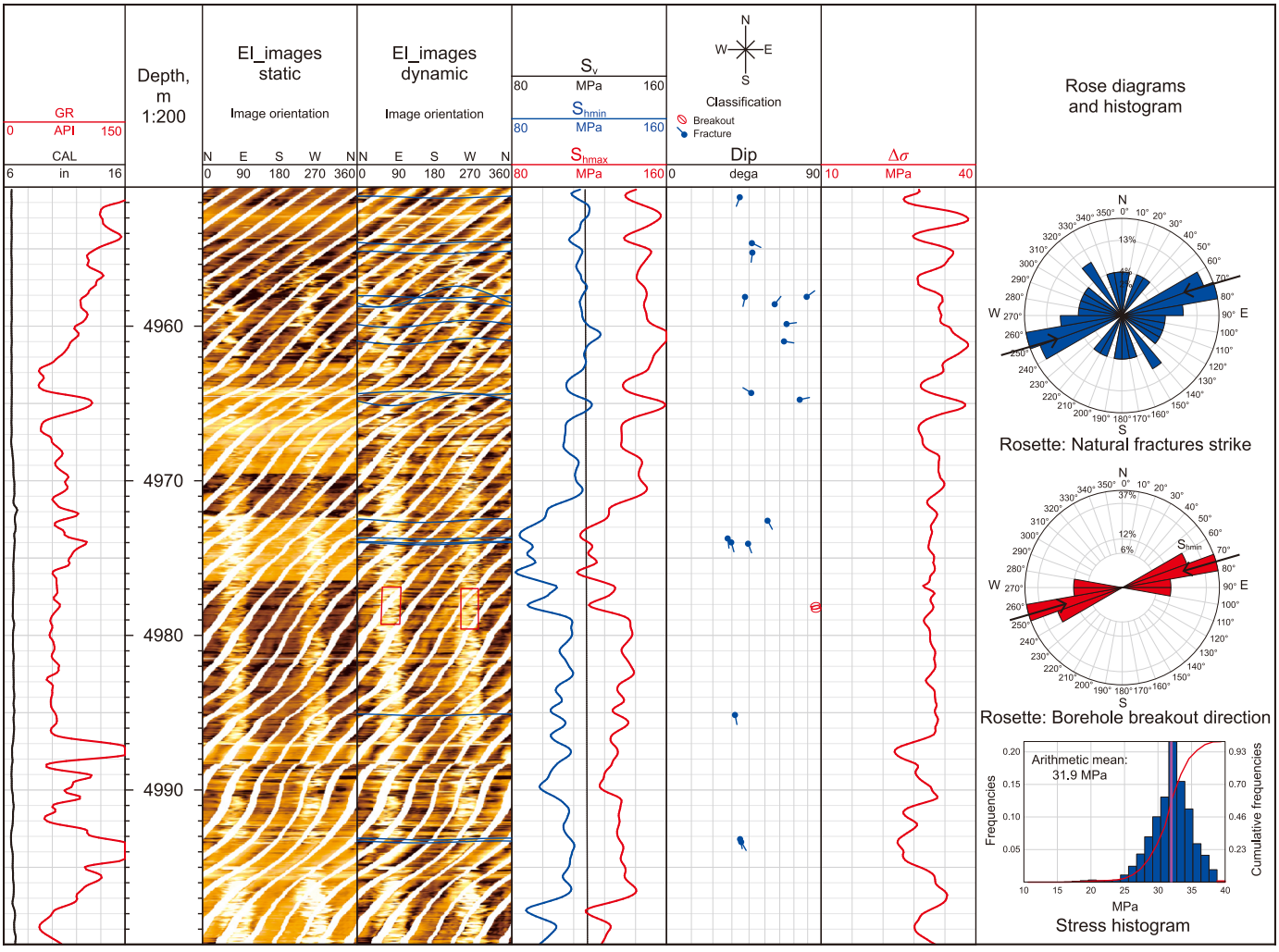

Fig. 15. Comprehensive evaluation of fracture effectiveness using image logs and in-situ stress for DB102 of Jurassic Ahe Formation in Kuqa Depression.

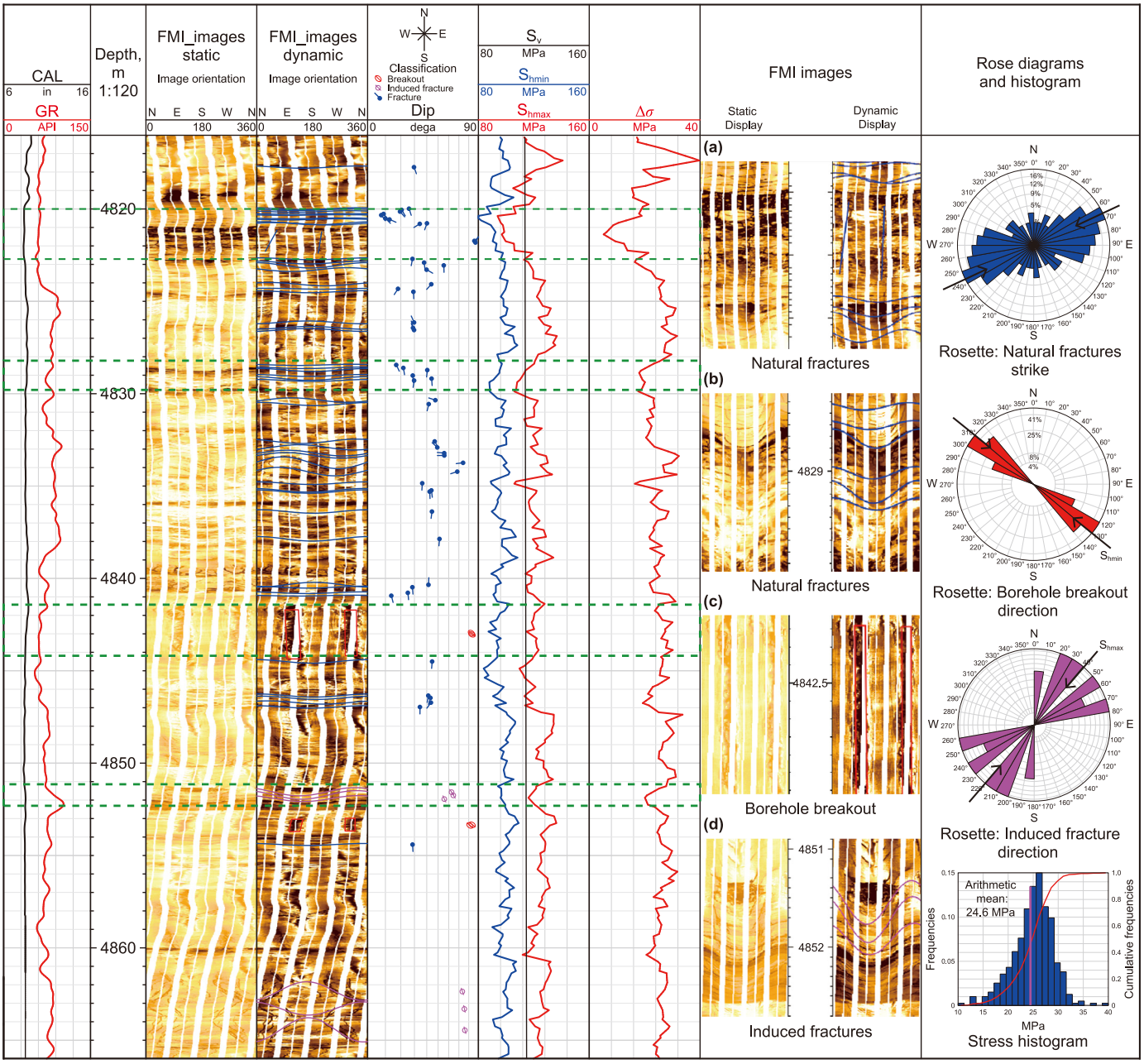

Fig. 16. Comprehensive evaluation of fracture effectiveness using image logs and in-situ stress for DX1 of Jurassic Ahe Formation in Kuqa Depression.

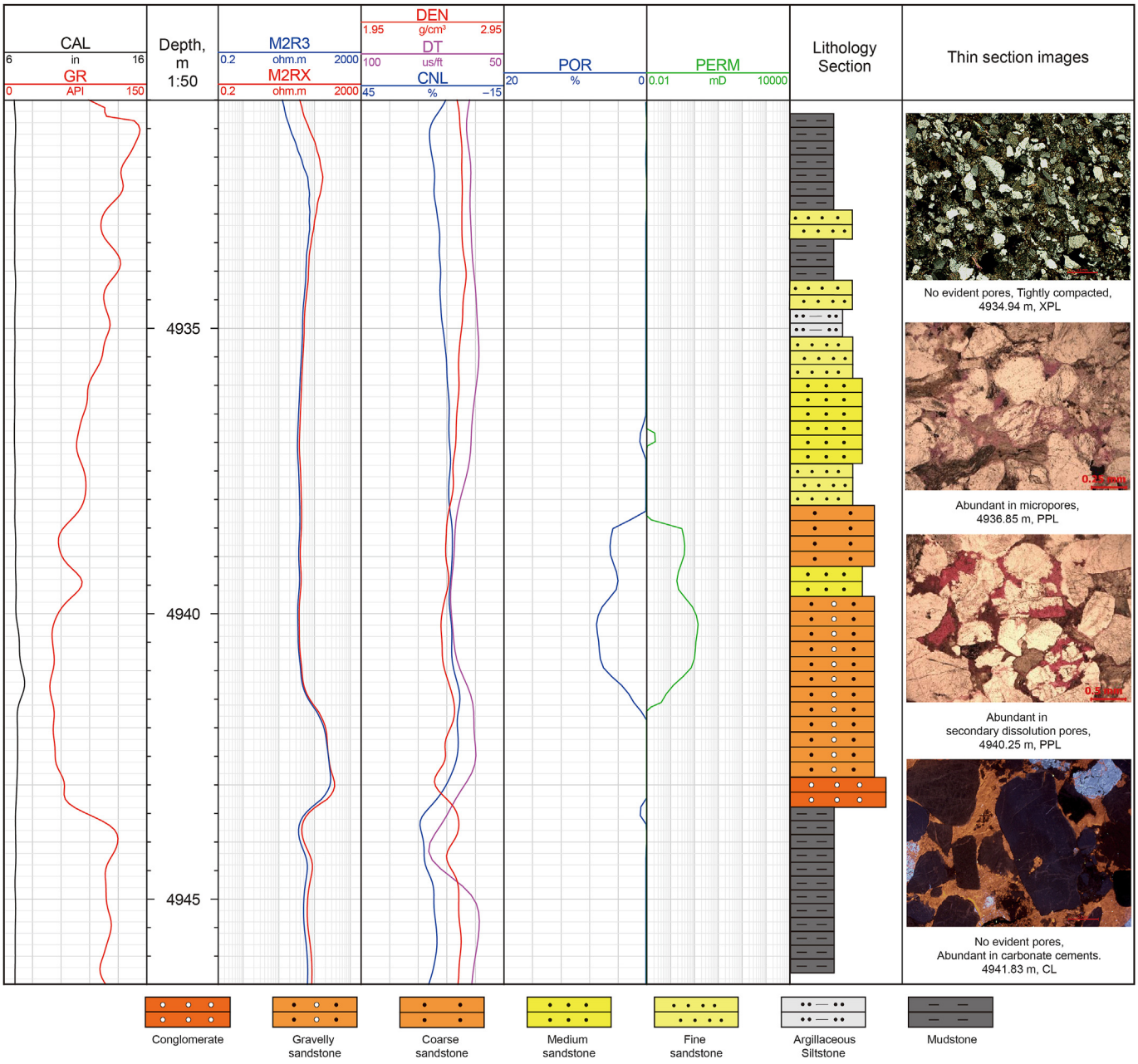

Fig. 17. The matrix pores controlled by sedimentation-diagenesis in Well DB102 of Jurassic Ahe Formation in Kuqa Depression.

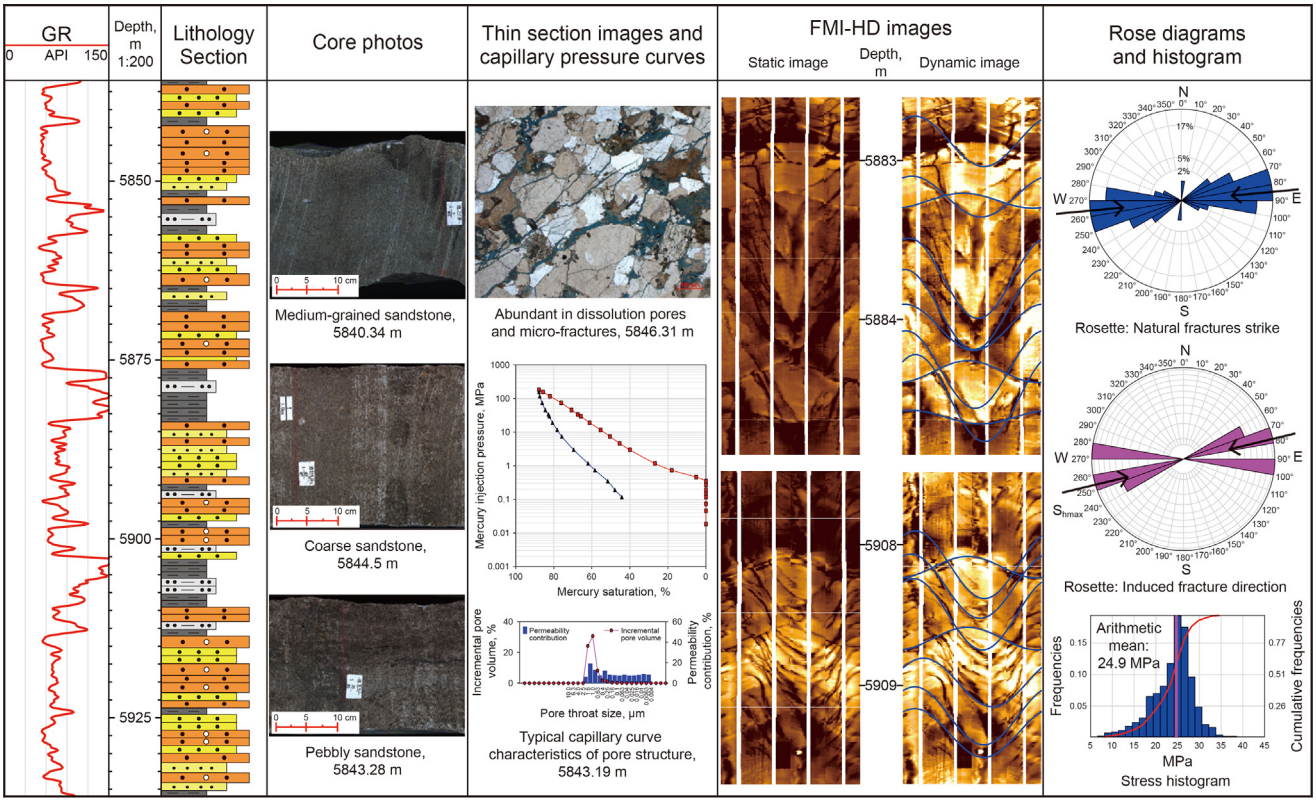

(a) Reservoir characteristics of low stress value zone

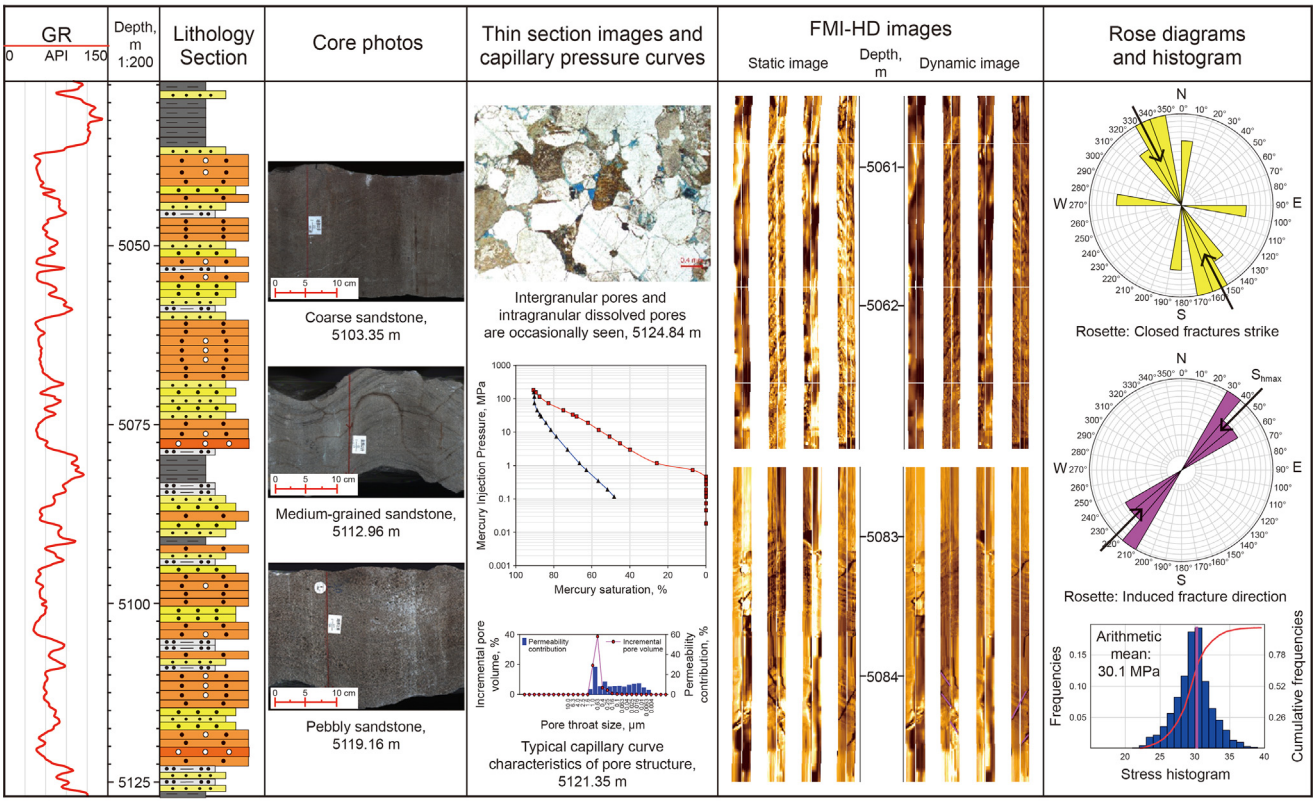

(b) Reservoir characteristics of high stress value zone

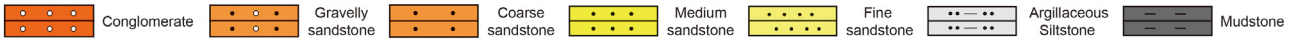

Fig. 18. The permeability and productivity controlled by fracture and in-situ stress of Jurassic Ahe Formation in Kuqa Depression.

Table 1
Oil test data of the seven wells in Figs. 13, 14, 16 and 17.

Well name	Depth intervals, m	Thickness, m	Choke width, mm	Daily oil production, m^3	Daily natural gas production, m^3	Drawdown pressure, MPa
DB5	5883.5–5925.5	42	4	3.36	90517	56.10
DX1	4898.0–4975.0	77	8	29.40	258662	29.46
DB102	4938.0–5099.0	161	6	2.85	13902	5.99
DB104	4768.0–4794.8	26.8	5	11.10	206528	61.80
DB103	4720.0–4890.0	170	Open	3.27	19262	
DB101	4867.0–4985.0	118	6	0	5851	4.84
DT2	5039.5–5839.5	800	7	0	1803	4.58

Note: Well DT2 is a large angle inclined well, and the target layer drilled looks thicker.

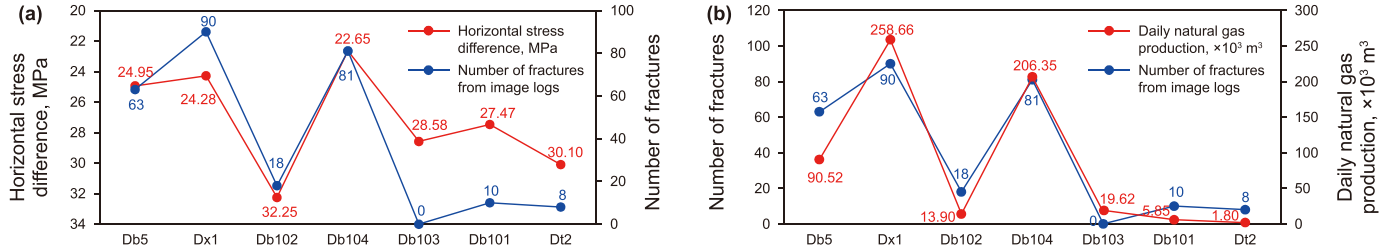

Fig. 19. The line chart of in-situ stress, fractures, and hydrocarbon productivity of Jurassic Ahe Formation in Kuqa Depression (Tarim Oilfield Company, 2023).

within the research area is illustrated in the line chart (Fig. 19). As shown in Fig. 19(a), in-situ stress closely influence the degree of fracture development and their effectiveness. The lower the stress value, the more developed the fractures become. Meanwhile, fractures can connect the matrix pores and form a network system, effectively improving the permeability, which is crucial for hydrocarbon productivity (Fig. 19(b)). Production data from multiple wells indicate a clear correlation between fractures and productivity, providing strong support for this viewpoint.

In summary, the varying degrees of natural fracture development and distinctions in-situ stress distribution are critical factors influencing the permeability and hydrocarbon productivity of the reservoir.

5.2. Reservoir quality evaluation and prediction

The combination of matrix pores and fractures in tight sandstone reservoirs is crucial for the formation of high-quality reservoirs, as well as for high and stable oil and gas production (Boutt et al., 2009; Radwan et al., 2021). In a compressional tectonic setting, controlled by sedimentation, diagenesis and tectonics, the reservoir quality and oil and gas productivity show obvious differences with the structural location (Fig. 20).

In the fault nose or fold core, the value of horizontal stress difference ($\Delta\sigma$) is relatively low, and the average $\Delta\sigma$ value of both DX1, DB104 and DB5 wells is less than 25 MPa, which are local weak stress area. Compaction is suppressed to a certain extent, fluid activity is frequent, dissolution is strengthened. Dissolution pores and microfractures are widely developed with great connectivity and permeability. Macroscopically, natural fractures are well-developed with good effectiveness (the angle between fracture strike and SH_{max} is less than 30°). The proportion of type I and type II reservoirs is relatively high, which is beneficial to oil and gas enrichment and high productivity (Fig. 20) (Table 1). In contrast, the wings of faults or folds and the footwalls of faults are areas of stress concentration with high $\Delta\sigma$ value (average around 30 MPa), showing a strong stress area. Thin section observations reveal that the grain contacts are dominated by long and concave-convex, pores and fractures are underdeveloped and the pores are sparsely and isolated distributed, indicating poor connectivity. This suggests that the reservoirs have undergone strong compaction. Macroscopically, the physical properties of reservoirs are poor, mainly type III and type IV, type I and type II reservoirs are underdeveloped, showing low hydrocarbon productivity or even dry layers (Fig. 20) (Table .1). The differential distribution of reservoir quality indicates the jointly control of sedimentation, diagenesis, and tectonics (fracture and in-situ stress) to the reservoir.

6. Conclusions

In a compressional tectonic setting, the reservoirs are controlled by sedimentation, diagenesis and tectonics. The sedimentary environment is the prerequisite and material basis for reservoir formation. The reservoir quality of tight sandstones in Jurassic Ahe Formation is environmentally selective, and the porosity and permeability increase with increasing grain sizes. Coarser grained sandstones with high depositional-energy have the best physical properties, while matrix-rich sediments with low depositional-energy, such as fine sandstone and mudstone, are easily to be tightly compacted, and have poor reservoir quality. Diagenesis is the key factor for the formation and development of reservoir matrix pores. Porosity decreases with compaction and cementation, and increases due to dissolution. Clay minerals filling pores result in micropores dominating the pore systems and a deterioration of pore structure. Microfractures formed by fracturing can promote dissolution and connect the matrix pores, effectively improving the seepage capacity of the reservoir. Pore reduction and fracture generation caused by tectonic compression are the key factors that affect the differences of reservoir quality. The result has shown that the in-situ stress has a significant control over the matrix physical properties and fracture effectiveness of the reservoir. The matrix physical properties are negatively correlated with the value of horizontal stress difference ($\Delta\sigma$). As the value of $\Delta\sigma$ increases, the pore structure becomes more complex, and the macroscopic reservoir quality becomes worse. The smaller the strike divergence between the natural fracture and SH_{max}, the lower the value of $\Delta\sigma$ in the fracture layers is, and the better the fracture effectiveness is.

Under the control of ternary factors on the reservoir, the matrix pores of the reservoirs are mainly controlled by sedimentary and

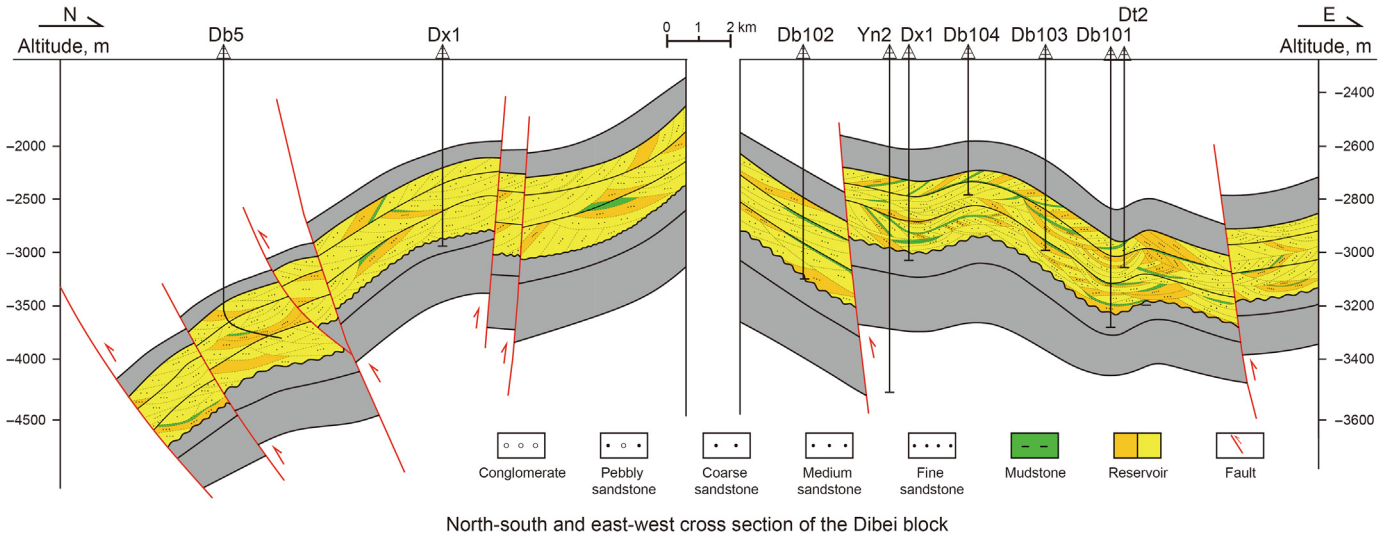

North-south and east-west cross section of the Dibei block

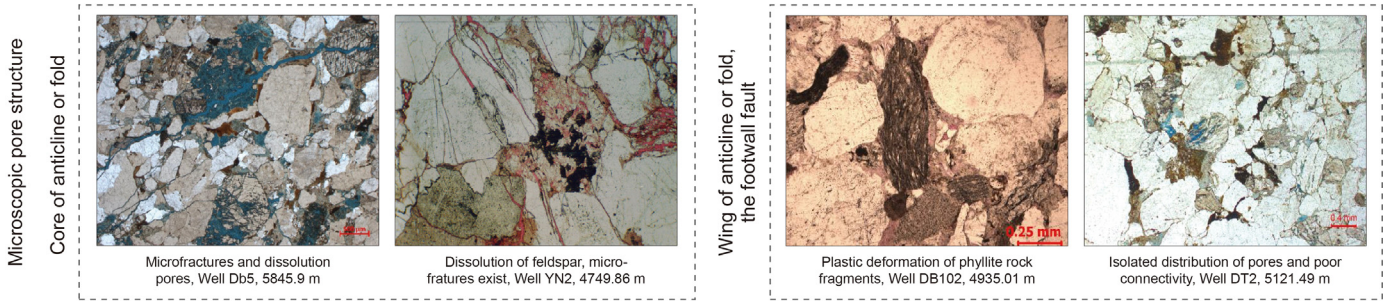

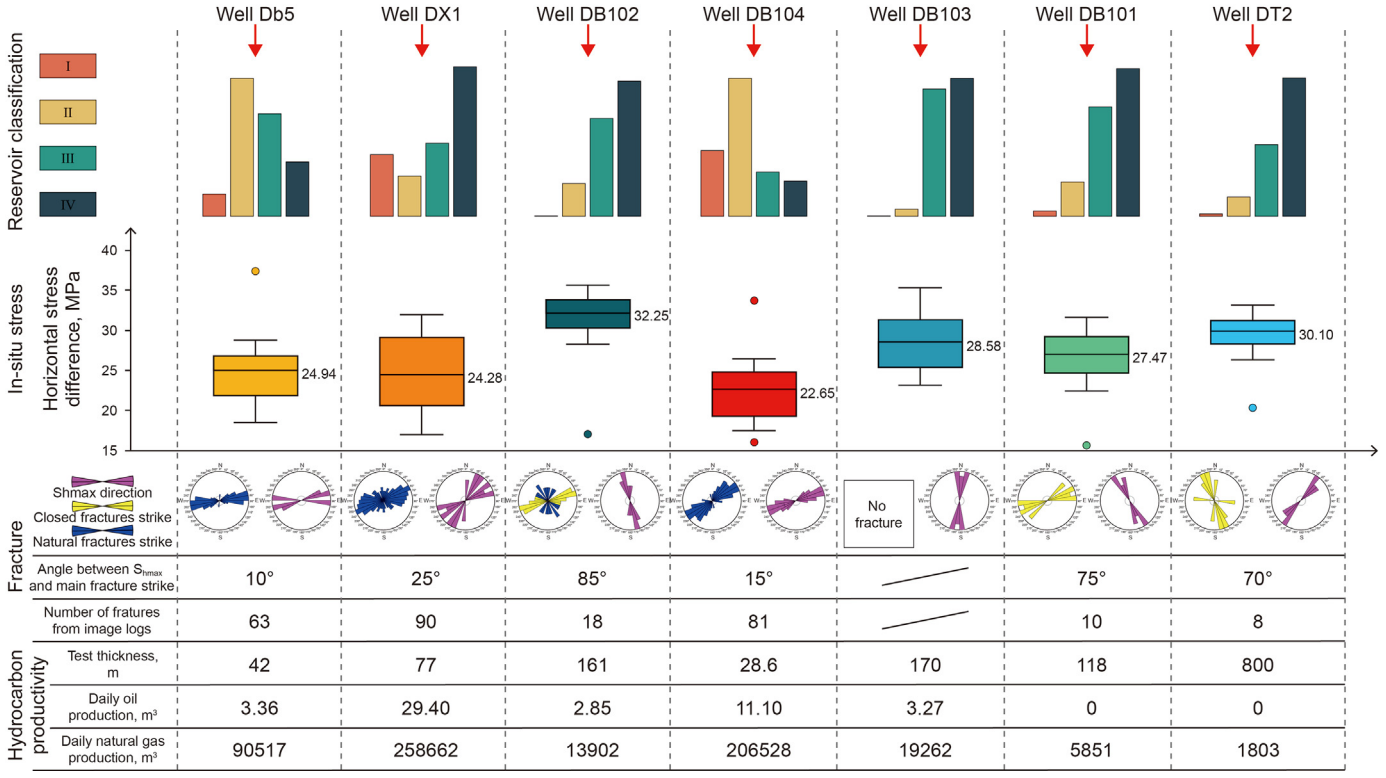

Fig. 20. Cross section of Dibei block and corresponding single well reservoir characteristics of Jurassic Ahe Formation in Kuqa Depression.

diagenetic factors. The sedimentary environment determines sandstone texture (grain size and sorting) and sand composition. Due to the initial difference of sedimentation affects subsequently diagenetic evolution, different intervals of the sandbodies may be modified by different diagenesis, affecting matrix pores. The superposition of high-energy sedimentary background and constructive diagenesis is conducive to the presence of matrix pores. Low-energy sedimentary background or destructive diagenesis leads to rare matrix pores and poor reservoir property. The varying degrees of natural fracture development and distinctions in-situ stress distribution are critical factors influencing the permeability and hydrocarbon productivity of the reservoir.

The reservoir quality and oil and gas productivity show obvious differences with the structural location. In the fault nose or fold core, there are local weak stress areas where fluid movement is frequent, intragranular dissolution pores and macro-microfractures are developed. Pores can be effectively preserved with good connectivity, and productivity is high. In the wing of the fold or the footwall fault, there are strong stress areas where fluid movement is weak, reservoir is tight, and pores and fractures are rare, and productivity is low. Reservoir quality in tight sandstones can be predicted by integrating sedimentation, diagenesis, and tectonics (fracture and in-situ stress) in a compressional tectonic setting.

CRediT authorship contribution statement

Dong Li: Writing – review & editing, Writing – original draft, Software, Methodology, Conceptualization, Validation, Methodology, Writing – review & editing. **Gui-Wen Wang:** Writing – review & editing, Supervision, Methodology, Conceptualization. **Kang Bie:** Resources, Project administration, Investigation, Data curation. **Jin Lai:** Writing – review & editing, Visualization, Investigation. **Song Wang:** Software, Validation, Visualization. **Hai-Hua Qiu:** Project administration, Data curation, Formal analysis. **Hong-Bo Guo:** Validation, Data curation, Project administration. **Fei Zhao:** Software, Methodology, Validation. **Xing Zhao:** Investigation, Formal analysis, Software. **Qi-Xuan Fan:** Investigation, Validation, Visualization.

Declaration of competing interest

The authors declare that they have no known competing financial interests or personal relationships that could have appeared to influence the work reported in this paper.

Acknowledgments

This work is financially supported by Science Foundation of China University of Petroleum, Beijing (No. 2462023QNXZ010, No. 2462023XKBH012, No. 2462024XKBH009) and China Postdoctoral Science Foundation (No. 2024M753612, No. GZC20233101). The authors would like to express their sincere thanks to the PetroChina Tarim Oilfield Company for their assistance in providing the information, and for their technical input to this work. We are also grateful to the four reviewers, whose comments improved the manuscript.

References

Almansour, A., Laubach, S.E., Bickel, J.E., et al., 2020. Value of Information analysis of a fracture prediction method. SPE Reservoir Eval. Eng. 23 (3), 811–823. https://doi.org/10.2118/198906-PA.

Ameen, M.S., MacPherson, K., Al-Marhoon, M.I., et al., 2012. Diverse fracture properties and their impact on performance in conventional and tight-gas reservoirs, Saudi Arabia: the Unayzah, South Haradh case study. AAPG Bull. 96 (3), 459–492. https://doi.org/10.1306/06011110148.

Baker, J.C., 1991. Diagenesis and reservoir quality of the aldebaran sandstone, denison trough, east-central queensland, Australia. Sedimentology 38, 819–838. https://doi.org/10.1111/j.1365-3091.1991.tb01874.x.

Baqués, V., Ukar, E., Laubach, S.E., et al., 2020. Fracture, dissolution, and cementation events in ordovician carbonate reservoirs, Tarim Basin, NW China. Geofluids 2020 (1), 9037429. https://doi.org/10.1155/2020/9037429.

Bjørlykke, K., 2014. Relationships between depositional environments, burial history and rock properties. Some principal aspects of diagenetic process in sedimentary basins. Sediment. Geol. 301, 1–14. https://doi.org/10.1016/j.sedgeo.2013.12.002.

Bloch, S., Lander, R.H., Bonnell, L., 2002. Anomalously high porosity and permeability in deeply buried sandstone reservoirs: origin and predictability. AAPG Bull. 86 (2), 301–328. https://doi.org/10.1306/61eedabc-173e-11d7-8645000102c1865d.

Boutt, D.F., Goodwin, L., McPherson, B.J., 2009. Role of permeability and storage in the initiation and propagation of natural hydraulic fractures. Water Resour. Res. 45 (5), 1–18. https://doi.org/10.1029/2007wr006557.

Brandes, C., Tanner, D., 2020. Fault mechanics and earthquakes. In: Tanner, D., Brandes, C. (Eds.), Understanding Faults. Elsevier, pp. 11–80. https://doi.org/10.1016/B978-0-12-815985-9.00002-3.

Cui, Y., Wang, G., Jones, S.J., et al., 2017. Prediction of diagenetic facies using well logs—a case study from the upper Triassic Yanchang Formation, Ordos Basin, China. Mar. Petrol. Geol. 81, 50–65. https://doi.org/10.1016/j.marpetgeo.2017.01.001.

Del Sole, L., Antonellini, M., Soliva, R., et al., 2020. Structural control on fluid flow and shallow diagenesis: insights from calcite cementation along deformation bands in porous sandstones. Solid Earth 11 (6), 2169–2195. https://doi.org/10.5194/se-11-2169-2020.

Dixit, N.C., Hanks, C.L., Wallace, W.K., et al., 2017. In-situ stress variations associated with regional changes in tectonic setting, northeastern Brooks Range and eastern North Slope of Alaska. AAPG Bull. 101 (3), 343–360. https://doi.org/10.1306/08051616013.

Dutton, S.P., Loucks, R.G., 2010. Diagenetic controls on evolution of porosity and permeability in lower Tertiary Wilcox sandstones from shallow to ultradeep (200–6700 m) burial, Gulf of Mexico Basin, USA. Mar. Petrol. Geol. 27 (1), 69–81. https://doi.org/10.1016/j.marpetgeo.2009.08.008.

Eaton, B.A., 1969. Fracture gradient prediction and its application in oilfield operations. J. Petrol. Technol. 246, 1353–1360. https://doi.org/10.2118/2163-PA.

Feng, J., Ren, Q., Xu, K., 2018. Quantitative prediction of fracture distribution using geomechanical method within Kuqa Depression, Tarim Basin, NW China. J. Petrol. Sci. Eng. 162, 22–34. https://doi.org/10.1016/j.petrol.2017.12.006.

Feng, W., Gao, F., Zhang, C., et al., 2024. Sedimentary architecture of a sandy braided river: insights from a flume experiment. Petrol. Sci. https://doi.org/10.1016/j.petsci.2024.07.016 (in press).

Folk, R.L., 1980. Petrology of Sedimentary Rocks. Hemphill Publishing Company, Austin, Texas, p. 182.

Grollimund, B., Zoback, M.D., Wiprut, D.J., et al., 2001. Stress orientation, pore pressure and least priciple stress in the Norwegian sector of the North Sea. Petrol. Geosci. 7, 173–180. https://doi.org/10.1144/petgeo.7.2.173.

Henares, S., Caracciolo, L., Cultrone, G., et al., 2014. The role of diagenesis and depositional facies on pore system evolution in a Triassic outcrop analogue (SE Spain). Mar. Petrol. Geol. 51, 136–151. https://doi.org/10.1016/j.marpetgeo.2013.12.004.

Higgs, K.E., Zwingmann, H., Reyes, A.G., et al., 2007. Diagenesis, porosity evolution, and petroleum emplacement in tight gas reservoirs, Taranaki basin, New Zealand. J. Sediment. Res. 77, 1003–1025. https://doi.org/10.2110/jsr.2007.095.

Higgs, K.E., Crouch, E.M., Raine, J.I., 2017. An interdisciplinary approach to reservoir characterisation; an example from the early to middle Eocene Kaimiro Formation, Taranaki Basin, New Zealand. Mar. Petrol. Geol. 86, 111–139. https://doi.org/10.1016/j.marpetgeo.2017.05.018.

Iqbal, O., Ahmad, M., Kadir, A., 2018. Effective evaluation of shale gas reservoirs by means of an integrated approach to petrophysics and geomechanics for the optimization of hydraulic fracturing: a case study of the Permian Roseneath and Murteree Shale Gas reservoirs, Cooper Basin, Australia. J. Nat. Gas Sci. Eng. 58, 34–58. https://doi.org/10.1016/j.jngse.2018.07.017.

Jia, C., 2007. The characteristics of intra-continental deformation and hydrocarbon distribution controlled by the Himalayan tectonic movements in China. Earth Sci. Front. 14 (4), 96–104. https://doi.org/10.1016/S1872-5791(07)60030-X.

Jiang, L., Hu, A., Ou, Y., et al., 2023. Diagenetic evolution and effects on reservoir development of the dengying and longwangmiao formations, central sichuan basin, southwestern China. Petrol. Sci. 20, 3379–3393. https://doi.org/10.1016/j.petsci.2023.09.025.

Ju, W., Wang, K., 2018. A preliminary study of the present-day in-situ stress state in the Ahe tight gas reservoir, Dibei Gasfield, Kuqa Depression. Mar. Petrol. Geol. 96, 154–165. https://doi.org/10.1016/j.marpetgeo.2018.05.036.

Ju, W., Shen, J., Qin, Y., et al., 2017. In-situ stress state in the Linxing region, eastern Ordos Basin, China: implications for unconventional gas exploration and production. Mar. Petrol. Geol. 86, 66–78. https://doi.org/10.1016/j.marpetgeo.2017.05.026.

Lai, J., Wang, G., Ran, Y., et al., 2015. Predictive distribution of high-quality reservoirs of tight gas sandstones by linking diagenesis to depositional facies: evidences from Xu-2 sandstones in Penglai area of central Sichuan basin, China. J. Nat. Gas Sci. Eng. 23, 97–111. https://doi.org/10.1016/j.jngse.2015.01.026.

Lai, J., Wang, G., Cao, J., et al., 2018. Investigation of pore structure and petrophysical property in tight sandstones. Mar. Petrol. Geol. 91, 179–189. https://doi.org/

10.1016/j.marpetgeo.2017.12.024.
Lai, J., Li, D., Wang, G., et al., 2019. Earth stress and reservoir quality evaluation in high and steep structure: the Lower Cretaceous in the Kuqa Depression, Tarim Basin. China. Mar. Petrol. Geol. 101, 43–54. https://doi.org/10.1016/j.marpetgeo.2018.11.036.
Lai, J., Li, D., Ai, Y., et al., 2022. Structural diagenesis in ultra-deep tight sandstones in Kuqa depression, Tarim Basin, China. Solid Earth 13, 975–1002. https://doi.org/10.5194/se-13-975-2022.
Lai, J., Li, D., Bai, T., et al., 2023. Reservoir quality evaluation and prediction in ultra-deep tight sandstones in the Kuqa depression, China. J. Struct. Geol. 170, 104850. https://doi.org/10.1016/j.jsg.2023.104850.
Lai, J., Su, Y., Xiao, L., et al., 2024. Application of geophysical well logs in solving geologic issues: past, present and future prospect. Geosci. Front. 15, 101779. https://doi.org/10.1016/j.gsf.2024.101779.
Lan, H., Martin, C.D., Hu, B., 2010. Effect of heterogeneity of brittle rock on micro-mechanical extensile behavior during compression loading. J. Geophys. Res. Solid Earth 115 (B1), B01202. https://doi.org/10.1029/2009JB006496.
Laubach, S.E., Eichhubl, P., Hilgers, C., et al., 2010. Structural diagenesis. J. Struct. Geol. 32 (12), 1866–1872. https://doi.org/10.1016/j.jsg.2010.10.001.
Li, J.H., Li, B.B., Cheng, Q.Y., et al., 2021. Characterization of the fracture compressibility and its permeability for shale under the effects of proppant embedment and compaction: a preliminary study. Petrol. Sci. 19 (3), 1125–1138. https://doi.org/10.1016/j.petsci.2021.12.021.
Li, Z., Zhang, L., Yuan, W., et al., 2022. Logging identification for diagenetic facies of tight sandstone reservoirs: a case study in the lower Jurassic Ahe formation, Kuqa Depression of Tarim basin. Mar. Petrol. Geol. 139, 105601. https://doi.org/10.1016/j.marpetgeo.2022.105601.
Liu, J., Ding, W., Gu, Y., et al., 2018a. Methodology for predicting reservoir breakdown pressure and fracture opening pressure in low permeability reservoirs based on an in-situ stress simulation. Eng. Geol. 246, 222–232. https://doi.org/10.1016/j.enggeo.2018.09.010.
Liu, J., Ding, W., Yang, H., et al., 2018b. Quantitative prediction of fractures using the finite element method: a case study of the lower Silurian Longmaxi Formation in northern Guizhou, South China. J. Asian Earth Sci. 154, 397–418. https://doi.org/10.1016/j.jseaes.2017.12.038.
Lu, X., Liu, S., Li, W., et al., 2014. Geological and resource evaluation in tight sandstone gas plays of low exploration degree: a case study of Jurassic tight sandstone gas in east Kuqa Basin. Nat. Gas Geosci. 25 (2), 178–184. https://doi.org/10.11764/j.issn.1672-1926.2014.02.0178.
Maleki, S., Moradzadeh, A., Riabi, R.G., et al., 2014. Comparison of several different methods of in-situ stress determination. Int. J. Rock Mech. Min. Sci. 71 (71), 395–404. https://doi.org/10.1016/j.ijrmms.2014.07.010.
Massiot, C., Mcnamara, D.D., Lewis, B., 2015. Processing and analysis of high temperature geothermal acoustic borehole image logs in the Taupo volcanic zone, New Zealand. Geothermics 53, 190–201. https://doi.org/10.1016/j.geothermics.2014.05.010.
Neng, Y., Xie, H., Yin, H., et al., 2018. Effect of basement structure and salt tectonics on deformation styles along strike: an example from the Kuqa fold–thrust belt, West China. Tectonophysics 730, 114–131. https://doi.org/10.1016/j.tecto.2018.02.006.
Nguyen, B.T.T., Jones, S.J., Goulty, N.R., et al., 2013. The role of fluid pressure and diagenetic cements for porosity preservation in Triassic fluvial reservoirs of the Central Graben, North Sea. AAPG Bull. 97 (8), 1273–1302. https://doi.org/10.1306/01151311163.
Nian, T., Wang, G., Xiao, C., et al., 2016. The in situ stress determination from borehole image logs in the Kuqa Depression. J. Nat. Gas Sci. Eng. 34, 1077–1084. https://doi.org/10.1016/j.jngse.2016.08.005.
Oilfield Company, Tarim, 2023. Report of research on ultra-deep and complex oil and gas reservoirs in the foreland thrust belt (internal report). Research Institute of Petroleum Exploration and Development, Tarim Oilfield Company, CNPC 58–97.
Ozkan, A., Cumella, S.P., Milliken, K.L., et al., 2011. Prediction of lithofacies and reservoir quality using well logs, late cretaceous williams fork formation, mamm creek field, piceance basin, Colorado. AAPG Bull. 95 (10), 1699–1723. https://doi.org/10.1306/01191109143.
Pang, X., Wang, G., Kuang, L., et al., 2022. Prediction of multiscale laminae structure and reservoir quality in fine-grained sedimentary rocks: the Permian Lucaogou Formation in Jimusar Sag, Junggar Basin. Petrol. Sci. 19 (6), 2549–2571. https://doi.org/10.1016/j.petsci.2022.08.001.
Pang, X., Wang, G., Kuang, L., et al., 2024. Investigation of fluid types in shale oil reservoirs. Surv. Geophys. 45 (5), 1561–1594. https://doi.org/10.1007/s10712-024-09845-9.
Peacock, D.C.P., Nixon, C.W., Rotevatn, A., et al., 2016. Glossary of fault and other fracture networks. J. Struct. Geol. 92, 12–29. https://doi.org/10.1016/j.jsg.2016.09.008.
Radwan, A.A., Nabawy, B.S., Abdelmaksoud, A., et al., 2021. Integrated sedimentological and petrophysical characterization for clastic reservoirs: a case study from New Zealand. J. Nat. Gas Sci. Eng. 88, 103797. https://doi.org/10.1016/j.jngse.2021.103797.
Rajabi, M., Tingay, M., Heidbach, O., 2016. The present-day state of tectonic stress in the darling basin, Australia: implications for exploration and production. Mar. Petrol. Geol. 77, 776–790. https://doi.org/10.1016/j.marpetgeo.2016.07.021.
Ramm, M., 2000. Reservoir quality and its relationship to facies and provenance in Middle to Upper Jurassic sequences, northeastern North Sea. Clay Miner. 35, 77–94. https://doi.org/10.1180/000985500546747.
Ren, Q., Jin, Q., Feng, J., et al., 2020. Geomechanical models for the quantitatively prediction of multi-scale fracture distribution in carbonate reservoirs. J. Pet. Sci. Eng. 195, 107942. https://doi.org/10.1016/j.jsg.2020.104033.
Ren, Q., Gao, J., Jiang, R., et al., 2024. Formation mechanism of fault accommodation zones under combined stress in graben basin: implications from geomechanical modeling. Petrol. Sci. 21, 54–76. https://doi.org/10.1016/j.petsci.2023.08.021.
Rezaee, M.R., Lemon, N.M., 1996. Influence of depositional environment on diagenesis and reservoir quality Tirrawarra sandstone reservoir, southern Cooper basin, Australia. J. Petrol. Geol. 19 (4), 369–391. https://doi.org/10.1111/j.1747-5457.1996.tb00445.x.
Rodrigues, R.S., Alves da Silva, F.C., Córdoba, V.C., 2021. Evolution of deformation bands, insights from structural diagenesis. J. Struct. Geol. 143, 104257. https://doi.org/10.1016/j.jsg.2020.104257.
Salem, A.M., Ketzer, J.M., Morad, S., et al., 2005. Diagenesis and reservoir-quality evolution of incised-valley sandstones: evidence from the Abu Madi gas reservoirs (upper Miocene), the Nile delta basin, Egypt. J. Sediment. Res. 75, 572–584. https://doi.org/10.2110/jsr.2005.047.
Shen, Y., Lü, X., Guo, S., et al., 2017. Effective evaluation of gas migration in deep and ultra-deep tight sandstone reservoirs of Keshen structural belt, Kuqa Depression. J. Nat. Gas Sci. Eng. 46, 119–131. https://doi.org/10.1016/j.jngse.2017.06.033.
Shi, C., Xu, A., Wei, H., et al., 2020. Quantitative characterization on the clastic reservoir destruction by tectonic compression: a case study of the Jurassic Ahe Formation in Yiqikelike structural belt Kuqa Depression. Acta Pet. Sin. 41 (2), 205–215. https://doi.org/10.7623/syxb202002006 (in Chinese).
Su, Y., Lai, J., Dang, W., et al., 2024. Pore structure characterization and reservoir quality prediction in deep and ultra-deep tight sandstones by integrating image and NMR logs. J. Asian Earth Sci. 272, 106232. https://doi.org/10.1016/j.jseaes.2024.106232.
Tang, Y., Yang, X., Xie, H., et al., 2021. Tight gas reservoir characteristics and exploration potential of jurassic Ahe Formation in Kuqa depression, Tarim Basin. China pet. Explor 26 (4), 113–124. https://doi.org/10.3969/j.issn.1672-7703.2021.04.009 (in Chinese).
Taylor, T.R., Giles, M.R., Hathon, L.A., et al., 2010. Sandstone diagenesis and reservoir quality prediction: models, myths, and reality. AAPG Bull. 94 (8), 1093–1132. https://doi.org/10.1306/04211009123.
Tingay, M.R.P., Hillis, R.R., Morley, C.K., et al., 2009. Present-day stress and neotectonics of Brunei: implications for petroleum exploration and production. AAPG Bull. 93, 75–100. https://doi.org/10.1306/08080808031.
Vandeginste, V., Swennen, R., Allaeys, M., et al., 2012. Challenges of structural diagenesis in foreland fold-and-thrust belts: a case study on paleofluid flow in the Canadian Rocky Mountains West of Calgary. Mar. Petrol. Geol. 35, 235–251. https://doi.org/10.1016/j.marpetgeo.2012.02.014.
Verweij, J.M., Boxem, T.A.P., Nelskamp, S., 2016. 3D spatial variation in vertical stress in on- and offshore Netherlands; integration of density log measurements and basin modeling results. Mar. Petrol. Geol. 78, 870–882. https://doi.org/10.1016/j.marpetgeo.2016.06.016.
Wang, K., Zhang, R., Yu, C., et al., 2020. Characteristics and controlling factors of jurassic Ahe reservoir of the northern tectonic belt, Kuqa Depression, Tarim Basin. Nat. Sci. Geosci. 31, 623–635. https://doi.org/10.11764/j.issn.1672-1926.2020.04.005 (in Chinese).
Wang, K., Zhang, R., Tang, Y., et al., 2022. Structural diagenesis and reservoir prediction of lower jurassic Ahe Formation in the northern structural belt of Kuqa depression. Acta Pet. Sin. 43 (7), 925–940. https://doi.org/10.7623/syxb202207004 (in Chinese).
Wang, Q., Zhang, R., Yang, X., et al., 2022. Major breakthrough and geological significance of tight sandstone gas exploration in Jurassic Ahe Formation in Dibei area, eastern Kuqa Depression. Acta Pet. Sin. 43 (8), 1049–1064. https://doi.org/10.7623/syxb202208002 (in Chinese).
Wang, S., Wang, G., Li, D., et al., 2022. Comparison between double caliper, imaging logs, and array sonic log for determining the in-situ stress direction: a case study from the ultra-deep fractured tight sandstone reservoirs, the Cretaceous Bashijiqike Formation in Keshen8 region of Kuqa Depression, Tarim Basin, China. Petrol. Sci. 19 (6), 2601–2617. https://doi.org/10.1016/j.petsci.2022.08.035.
Wei, G., Wang, K., Zhang, R., et al., 2022. Structural diagenesis and high-quality reservoir prediction of tight sandstones: a case study of the Jurassic Ahe Formation of the Dibei gas reservoir, Kuqa Depression, Tarim basin, NW China. J. Asian Earth Sci. 239, 105399. https://doi.org/10.1016/j.jseaes.2022.105399.
Wilson, T.H., Smith, V., Brown, A., 2015. Developing a model discrete fracture network, drilling, and enhanced oil recovery strategy in an unconventional naturally fractured reservoir using integrated field, image log, and three-dimensional seismic data. AAPG Bull. 99 (4), 735–762. https://doi.org/10.1306/10031414015.
Xi, K., Cao, Y., Haile, B.G., et al., 2016. How does the pore-throat size control the reservoir quality and oiliness of tight sandstones? The case of the Lower Cretaceous Quantou Formation in the southern Songliao Basin. China. Mar. Petrol. Geol. 76, 1–15. https://doi.org/10.1016/j.marpetgeo.2016.05.001.
Xin, Y., Wang, G., Liu, B., et al., 2022. Pore structure evaluation in ultra-deep tight sandstones using NMR measurements and fractal analysis. J. Pet. Sci. Eng. 211, 110180. https://doi.org/10.1016/j.petrol.2022.110180.
Zeng, L., Wang, H., Gong, L., et al., 2010. Impacts of the tectonic stress field on natural gas migration and accumulation: a case study of the Kuqa Depression in the Tarim Basin. China. Mar. Petrol. Geol. 27, 1616–1627. https://doi.org/10.1016/j.marpetgeo.2010.04.010.

Zeng, Q., Mo, T., Zhao, J., et al., 2020. Characteristics, genetic mechanism and oil & gas exploration significance of high-quality sandstone reservoirs deeper than 7000 m: A case study of the Bashijiqike Formation of Lower Cretaceous in the Kuqa Depression, NW China. Nat. Gas. Ind. B 7 (4), 317–327. https://doi.org/10.1016/j.ngib.2020.01.003.

Zeng, L., Song, Y., Liu, G., et al., 2023. Natural fractures in ultra-deep reservoirs of China: a review. J. Struct. Geol. 175, 104954. https://doi.org/10.1016/j.jsg.2023.104954.

Zhang, Y., Pe-Piper, G., Piper, D.J.W., 2015. How sandstone porosity and permeability vary with diagenetic minerals in the Scotian Basin, offshore Eastern Canada: implications for reservoir quality. Mar. Petrol. Geol. 63, 28–45. https://doi.org/10.1016/j.marpetgeo.2015.02.007.

Zhang, R., Yang, H., Wei, H., et al., 2020. Sandstone characteristics and hydrocarbon exploration significance of the Middle-Lower Jurassic of the centraleastern part of the northern tectonic belt of the Kuqa Depression, Tarim Basin, China. J. Nat. Gas Geosci. 5 (2), 81–90. https://doi.org/10.1016/j.jnggs.2020.03.001.

Zhang, R., Wei, G., Wang, K., et al., 2021. Tectonic thrust nappe activity and sandstone rock response characteristics in foreland thrust belt: a case study of Middle and Lower Jurassic, Kuqa Depression, Tarim Basin. Acta Pet. Sin. 37 (7), 2256–2270. https://doi.org/10.18654/1000-0569/2021.07.17 (in Chinese).

Zoback, M., Barton, C., Brudy, M., et al., 2003. Determination of stress orientation and magnitude in deep wells. Int. J. Rock Mech. Min. Sci. 40, 1049–1076. https://doi.org/10.1016/j.ijrmms.2003.07.001.

Zou, C., Zhu, R., Liu, K., et al., 2012. Tight gas sandstone reservoirs in China: characteristics and recognition criteria. J. Pet. Sci. Eng. 88–89, 82–91. https://doi.org/10.1016/j.petrol.2012.02.001.